

NASA TM X-304



GPO PRICE \$ _____

CFSTI PRICE(S) \$ _____

Hard copy (HC) 2.50

Microfiche (MF) .50

653 July 66

TECHNICAL MEMORANDUM

X-304 DECLASSIFIED- AUTHORITY
US 1166

DROBKA TO LEBOW MEMO DATED
APRIL 19, 1966

THE TRANSONIC AERODYNAMIC CHARACTERISTICS OF
TWO VARIABLE-SWEEP AIRPLANE CONFIGURATIONS CAPABLE OF
LOW-LEVEL SUPERSONIC ATTACK

By Ralph P. Bielat, A. Warner Robins,
and William J. Alford, Jr.

Langley Research Center
Langley Field, Va.

Declassified by authority of NASA
Classification Change Notice No. 44
Dated 11/15/96

N 66 31729

(ACCESSION NUMBER)

(THRU)

55

(PAGES)

1

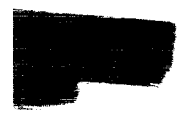
(CODE)

TM X-304

(NASA CR OR TMX CR AD NUMBER)

01

(CATEGORY)



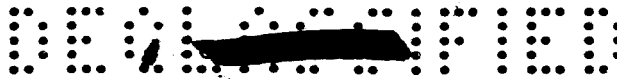
NATIONAL AERONAUTICS AND SPACE ADMINISTRATION

WASHINGTON

August 1960



FACILITY FORM 602



NATIONAL AERONAUTICS AND SPACE ADMINISTRATION

TECHNICAL MEMORANDUM X-304

THE TRANSONIC AERODYNAMIC CHARACTERISTICS OF
TWO VARIABLE-SWEEP AIRPLANE CONFIGURATIONS CAPABLE OF
LOW-LEVEL SUPERSONIC ATTACK*

By Ralph P. Bielat, A. Warner Robins,
and William J. Alford, Jr.

DECLASSIFIED - AUTHORITY
US 1166
DROBKA TO LEBOW MEMO DATED
APRIL 19, 1966

Declassified by authority of NASA
Classification Change Notices No. 64 SUMMARY
Dated ** 6/1/66 ---

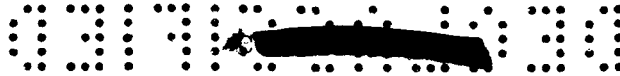
The aerodynamic characteristics of two variable-sweep airplane configurations capable of low-level supersonic attack have been investigated. The wind-tunnel results have indicated that the configurations with maximum wing sweep had high Mach numbers for the drag rise and low values of the zero-lift drag-rise characteristics. For the configuration with 25° wing sweep, high values of maximum lift-drag ratio were indicated.

INTRODUCTION

The National Aeronautics and Space Administration has been engaged in wind-tunnel research directed toward the development of a multimission military airplane which might combine long subsonic range for ferry and loiter purposes, efficient supersonic performance for high-altitude attack missions, and good landing and take-off characteristics for carrier and short-field operation. Since it appeared highly improbable that a fixed-wing aircraft could accomplish all of these missions satisfactorily, the research was directed towards variable-sweep configurations. Inasmuch as the feasibility of in-flight sweep variations had been satisfactorily demonstrated in the past with the X-5 and XF10F airplanes, research was directed towards an aerodynamic solution to the problem of reducing stability variations and thereby eliminating the fore-and-aft wing translation occurring in the previous aircraft and to the use of the higher sweeps dictated by the supersonic attack requirement. The results of this study are presented in references 1 to 6 and



L
1
1
5
0



indicate that by careful planform and pivot-point selection, a configuration having essentially the same longitudinal stability at 25° and 75° sweep and providing large changes in aspect ratio could be developed.

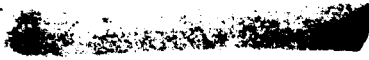
Recently, the possibility of adding another mission - one requiring a rather long range of low-level supersonic flight - has been studied. During this study, in which some ten configurations were considered, the desirability of extending the sweep range so that a large portion of the wing could be confined within or on top of the fuselage became evident. This arrangement would allow considerable reduction in wave drag, friction drag, and gust accelerations and, because of the high dynamic pressures encountered (resulting in low angles of attack), would incur only minor penalties in drag due to lift. The purpose of this paper is to present the results of transonic wind-tunnel studies of two of these configurations having variable-sweep wings capable of being rotated to sweep angles sufficiently high to enable a large portion of the wing to be on top of the fuselage. In order to assure low values of wave drag, the transonic area-rule concept of reference 7 was used in determining the fuselage contours.

The first configuration (referred to herein as configuration VII) has the wing pivot located within the fuselage and thereby allows an extremely large portion of the wing friction drag to be eliminated by sweeping. The second configuration (referred to herein as configuration VIII) had the pivot located at approximately the 25-percent-span position (of the unswept condition) in an attempt to reduce the large stability changes anticipated with the inboard pivot of configuration VII. (See refs. 1 and 8.) Results were obtained in the Langley 8-foot transonic pressure tunnel at Mach numbers ranging from 0.60 to 1.20 with the wings in the fully sweptback condition. The only other wing-sweep position tested was the 25° position for configuration VIII at Mach numbers from 0.60 to 0.96.

SYMBOLS

The data are referred to the wind axes and are based on an area of 1 square foot and a reference chord of 1 foot. The pitching moments have been referred to an axis which is located at the wing-pivot axis. The coefficients and symbols used herein are defined as follows:

A	cross-sectional area, sq ft
c	reference chord, 1.00 ft



L
1
1
5
0

DEFINITIONS

- C_D drag coefficient, $\frac{\text{Drag}}{qS}$
- $C_{D,o}$ drag coefficient at zero lift
- $\Delta C_{D,o}$ incremental drag rise at zero lift, $(C_{D,o})_M - (C_{D,o})_{M=0.80}$
- $C_{D,i}$ internal-drag coefficient of ducts, $\frac{\text{Internal drag}}{qS}$
- $C_{D,b}$ base-drag coefficient, $\frac{(\text{Base pressure})A_b}{qS}$
- C_L lift coefficient, $\frac{\text{Lift}}{qS}$
- $C_{L,(L/D)_{\max}}$ lift coefficient for $(L/D)_{\max}$
- $C_{L\alpha}$ lift-curve slope, $\frac{dC_L}{d\alpha}$
- C_m pitching-moment coefficient, $\frac{\text{Pitching moment}}{qSc}$
- C_{mC_L} pitching-moment-curve slope, $\frac{dC_m}{dC_L}$
- L/D lift-drag ratio
- M free-stream Mach number
- q free-stream dynamic pressure, $\frac{1}{2}\rho V^2$, lb/sq ft
- R Reynolds number based on $c = 1.00$ ft
- S reference area, 1.00 sq ft
- V velocity, ft/sec

L
1
1
5
0





α angle of attack referred to fuselage reference line, deg
 i_t stabilizer incidence referred to fuselage reference line, positive when trailing edge is down, deg
 ρ air density, slugs/cu ft
 w mass-flow rate, ρAV , lb-sec/ft

Subscripts:

b base
 t throat
 ∞ free stream
 max maximum

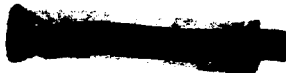
L
1
1
5
0

DESCRIPTION OF THE CONFIGURATIONS

General-arrangement drawings of the configurations are presented in figures 1, 2, and 3. Basic differences in the configurations are the maximum cross-sectional frontal areas and the location of the wing-pivot axes. Configuration VII has a maximum frontal area of 44.3 square feet, a wetted area of 2,777 square feet, and has an inboard wing-pivot location; whereas, configuration VIII has a reduced maximum frontal area of 40 square feet made possible by the outboard wing-pivot location and a wetted area of 2,990 square feet. Another feature of the outboard wing-pivot location is to reduce the stability variations during wing rotation. Configuration VIIA (fig. 2) consists essentially of a combination of configuration VII from the nose to fuselage station 56 feet (full-scale) and of configuration VIII from fuselage station 56 feet to fuselage station 81.5 feet (full-scale). The frontal area, wing planform, and wing-pivot location are the same as those for configuration VII and the empennage is the same as that for configuration VIII; however, the horizontal-tail location for configuration VIIA is farther forward in comparison with that for configuration VII.

Area Curves

Total-cross-sectional-area curves for the various configurations are shown in figures 4, 5, and 6. An equivalent free-stream tube area of 8.34 square feet, full-scale, (62 percent of maximum inlet capture area) was subtracted to account for the mass flow through the ducts.





These area curves, which were developed for a Mach number of 1, are compared with those for a Sears-Haack body of revolution with the maximum area at the midlength. The equivalent-body fineness ratio for configurations VII and VIIA was 10.84, as compared with the value of 11.43 for configuration VIII.

Wind-Tunnel Models

L
1
1
5
0
The models of the present investigation were 1/24 scale. Photographs of configurations VII, VIIA, and VIIA with reconnaissance pod are shown in figures 7, 8, and 9, respectively. Configuration VIII with the leading edge of the outer wing panel swept back 25° is shown in figure 10. The models were constructed primarily of plastic-impregnated fiber glass, steel, and aluminum alloy. No provisions were made to simulate the inner and outer wing-panel junctures on the models. It was necessary to modify the models at the aft end of the fuselages for the sting supports.


For tests with the wing extended on configuration VIII, the outer wing panel had a leading-edge sweepback angle of 25°. The streamwise airfoil section of the outer wing panel consisted of the upper half of an NACA 65₁A012 section with a leading-edge radius of approximately 0.26 percent of the chord.

The jet-engine inlets simulated on each model configuration were designed and constructed so as to provide the proper mass flow for a Mach number of 1.20. The variation of mass-flow ratio with angle of attack for the Mach number range of 0.60 to 1.20 is given in figure 11 for model configurations VII and VIII. The mass-flow ratio was based on the minimum inlet throat area ($A_t = 0.00742$ square foot per duct as measured on models) and it will be noted that the experimentally measured values at a Mach number of 1.20 correspond very closely to the design value of 0.97.

APPARATUS AND PROCEDURES

Tunnel

The investigation was made in the Langley 8-foot transonic pressure tunnel. This facility is rectangular in cross section with the upper and lower walls slotted longitudinally to allow continuous operation through the transonic speed region with negligible effects of choking and blockage. For the most part, the tunnel was operated at a stagnation pressure of one atmosphere; however, for configuration VIII with





the 25° sweptback wing, the stagnation pressure was lowered to approximately one-quarter atmosphere. The stagnation temperature and dewpoint were maintained at a level to preclude shock condensation effects.

Reynolds Number

The Reynolds number based on a characteristic length of 1 foot is shown in figure 12 as a function of test Mach number. The Reynolds number varied from 3.14×10^6 to 4.18×10^6 for configurations VII, VIIA, and VIII with wings swept back onto the fuselage. The Reynolds number varied from 0.86×10^6 to 1.09×10^6 for configuration VIII with the wing swept back 25°.

L
1
1
5
0

Measurements

Lift, drag, and pitching moment were determined by means of an electrical strain-gage balance located inside the fuselage. The measurements were taken over a small angle-of-attack range to define the zero-lift drag characteristics for the configurations with the wings swept back onto the fuselage and over an angle-of-attack range which would be sufficient to define the $(L/D)_{\max}$ characteristics for configuration VIII with the wing swept back 25°. The Mach number range varied from 0.60 to 1.20. Total-pressure and static-pressure measurements were taken at the duct exits to determine the mass-flow and internal-drag coefficient. The base pressure at the aft end of the fuselage and the balance chamber pressure were also determined.

All tests were conducted with fixed transition on the models according to the methods described in reference 9. The transition was fixed by applying 0.10-inch-wide strips of No. 80 carborundum grains around the fuselage 2 inches back from the nose, at the leading edge of the inlets, 0.25 inch rearward perpendicular to the leading edge of both surfaces of the wing, and at the 10-percent-chord location on all surfaces of the horizontal and vertical tails.

Corrections and Accuracy

No corrections to the free-stream Mach number and dynamic pressure for the effects of model and wake blockage are necessary for tests in the slotted test section of the Langley 8-foot transonic pressure tunnel (ref. 10). There is a range of Mach numbers above a Mach number of 1.00 where the data are affected by reflected compressions and expansions from the test-section boundary. From considerations of the results of reference 11, it is believed that for Mach numbers up to approximately 1.03



the effects of these disturbances on the measurements made in the present investigation would be negligible. No test data, however, are presented in the range ($M > 1.03$ and $M < 1.15$) where the reflected boundary disturbances impinged upon the models.

The drag data have been corrected for base pressure so that the drag corresponds to conditions where the base pressure is equal to the free-stream static pressure. The drag data have also been corrected for a buoyant force on the balance; this correction was obtained from measurements of the static pressure in the balance chamber. Typical plots of the total base-drag coefficient against angle of attack are given in figure 13. The internal drag has been also subtracted from the drag data to give a net external drag. The variation of the internal-drag coefficient with angle of attack is shown in figure 14. This drag coefficient is the total value for both nacelles.

No corrections for the forces and moments produced by the sting-support interference have been applied to the data. It is believed that the significant corrections would be limited to small increments in pitching moment and drag.

The angle of attack has been corrected for flow angularity and for the deflection of the sting-support system under load. The angle of attack is estimated to be accurate to within $\pm 0.1^\circ$.

The estimated consistency of the data at a Mach number of 0.90, based on the static calibrations and the repeatability of the data, is as follows:

C_L	± 0.002
C_D	± 0.0004
C_m	± 0.004

These errors would be inversely proportional to the dynamic pressure and, therefore, would be lower at the higher Mach numbers.

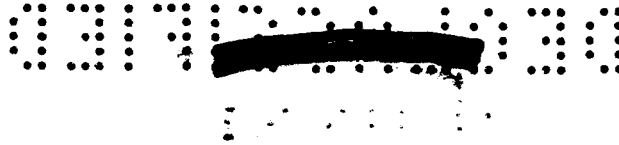
RESULTS AND DISCUSSION

The results of this investigation are presented in the following figures:

Figure

Aerodynamic characteristics of configuration VII ($i_t = 0^\circ$)	15
---	----





Figure

Aerodynamic characteristics of configuration VIIA ($i_t = 0^\circ$)	16
Aerodynamic characteristics of configuration VIIA with reconnaissance pod ($i_t = 0^\circ$)	17
Aerodynamic characteristics of configuration VIII	18
Comparisons of drag rise for configurations with maximum wing sweep	19
A comparison of lift-curve slopes for configurations with maximum wing sweep ($C_L = 0$)	20
A comparison of pitching-moment-curve slopes for configurations with maximum wing sweep ($C_L = 0$)	21
Aerodynamic characteristics of configuration VIII with wing swept back 25° ($i_t = 1.5^\circ$)	22
Variation of lift-drag ratio with lift coefficient at various Mach numbers for configuration VIII with wing swept back 25°	23
Variation with Mach number of maximum lift-drag ratio and lift coefficient for $(L/D)_{max}$ for configuration VIII with wing swept back 25°	24
Variation of lift-curve slope with Mach number for configura- tion VIII with wing swept back 25° ($C_L = 0.3$)	25
Variation of pitching-moment-curve slope with Mach number for configuration VIII with wing swept back 25° ($C_L = 0.3$)	26

Aerodynamic Characteristics of Configurations

With Maximum Wing Sweep

Drag characteristics.- A comparison of the drag characteristics at zero lift for configurations VII, VIIA, and VIII is presented in figure 19. The drag-rise Mach number increased from about 0.95 to 0.99 and the incremental drag rise at zero lift at a Mach number of 1.20 decreased approximately 27 percent for configuration VIII when compared with configuration VII. Configuration VIIA had a more favorable area distribution at the aft end compared with configuration VII (figs. 4 and 5) and, as a consequence, the drag characteristics for this configuration were intermediate between those of configurations VII and VIII. It should be noted that the zero-lift drag-rise characteristics of the three configurations were low and compare favorably with other configurations designed according to the area-rule principles of reference 7.

Longitudinal stability characteristics.- The lift-curve slopes measured near zero-lift coefficient for configurations VII, VIIA, and VIII are compared in figure 20. The values of $C_{L\alpha}$ were small and showed only



a slight variation throughout the Mach number range. The lift-curve slope for configuration VIII was somewhat higher than the values for configurations VII and VIIA as a result of the greater exposed wing area of configuration VIII caused by the outboard wing-pivot location.

The pitching-moment-curve slopes C_{mC_L} , measured near zero-lift coefficient, are given in figure 21 for the three configurations. In general, these data indicate that the values of C_{mC_L} became more positive (which represents a forward movement of the aerodynamic-center location) as the Mach number was increased to 1.20. An increase in stability of these configurations near a Mach number of 1.20 will be required in order to make safe operation at low levels. The configurations also indicated a positive shift of the pitching-moment coefficient at zero lift as the Mach number was increased to 1.20; this shift would relieve the trimming requirements. It will be noted, also, that modifying configuration VII to configuration VIIA had a destabilizing effect on the pitching-moment characteristics (figs. 15(c) and 16(c)) which was due to the forward location of the horizontal tail on configuration VIIA.

Aerodynamic Characteristics of Configuration VIII

With Wing Swept Back 25°

Drag characteristics.- The untrimmed lift-drag ratio characteristics for configuration VIII with the wing swept back 25° are shown in figure 23. The variation of the untrimmed $(L/D)_{max}$ and lift coefficient for $(L/D)_{max}$ with Mach number are given in figure 24. There was a large reduction in the values of $(L/D)_{max}$ as the Mach number was increased above the critical Mach number of about 0.82.

Longitudinal stability characteristics.- The variation with Mach number of the lift-curve slope and the pitching-moment-curve slope are presented in figures 25 and 26, respectively. It will be noted that $C_{L\alpha}$ increased abruptly above a Mach number of 0.85 and that the pitching-moment-curve slope C_{mC_L} indicates the usual rearward movement of the aerodynamic-center location with increase in Mach number.

CONCLUDING REMARKS

The aerodynamic characteristics of two variable-sweep airplane configurations capable of low-level supersonic attack have been investigated. The wind-tunnel results have indicated that the configurations



with maximum wing sweep had high Mach numbers for the drag rise and low values of the zero-lift drag-rise characteristics. For the configuration with 25° wing sweep, high values of maximum lift-drag ratio were indicated.

Langley Research Center,
National Aeronautics and Space Administration,
Langley Field, Va., May 5, 1960.

L
1
1
5
0



REFERENCES

1. Alford, William J., Jr., and Henderson, William P.: An Exploratory Investigation of the Low-Speed Aerodynamic Characteristics of Variable-Wing-Sweep Airplane Configurations. NASA TM X-142, 1959.
2. Alford, William J., Jr., Luoma, Arvo A., and Henderson, William P.: Wind-Tunnel Studies at Subsonic and Transonic Speeds of a Multiple-Mission Variable-Wing-Sweep Airplane Configuration. NASA TM X-206, 1959.
3. Spearman, M. Leroy, and Foster, Gerald V.: Stability and Control Characteristics at a Mach Number of 2.01 of a Variable-Wing-Sweep Configuration With Outboard Wing Panels Swept Back 75°. NASA TM X-32, 1959.
4. Spearman, M. Leroy, and Foster, Gerald V.: Effects of Various Modifications on the Supersonic Stability Characteristics of a Variable-Wing-Sweep Configuration at a Mach Number of 2.01. NASA TM X-260, 1960.
5. Foster, Gerald V.: Stability and Control Characteristics at Mach Numbers of 2.50, 3.00, and 3.71 of a Variable-Wing-Sweep Configuration With Outboard Wing Panels Swept Back 75°. NASA TM X-267, 1960.
6. Foster, Gerald V.: Effects of Spoiler-Slot-Deflector Control on the Aerodynamic Characteristics at a Mach Number of 2.01 of a Variable-Wing-Sweep Configuration With the Outer Wing Panels Swept Back 75°. NASA TM X-273, 1960.
7. Whitcomb, Richard T.: A Study of the Zero-Lift Drag-Rise Characteristics of Wing-Body Combinations Near the Speed of Sound. NACA Rep. 1273, 1956. (Supersedes NACA RM L52H08.)
8. Spencer, Bernard, Jr.: Stability and Control Characteristics at Low Subsonic Speeds of an Airplane Configuration Having Two Types of Variable-Sweep Wings. NASA TM X-303, 1960.
9. Braslow, Albert L., and Knox, Eugene C.: Simplified Method for Determination of Critical Height of Distributed Roughness Particles for Boundary-Layer Transition at Mach Numbers From 0 to 5. NACA TN 4363, 1958.

SECRET

- 10. Wright, Ray H., and Ward, Vernon G.: NACA Transonic Wind-Tunnel Test Sections. NACA Rep. 1231, 1955. (Supersedes NACA RM L8J06.)
- 11. Wright, Ray H., Ritchie, Virgil S., and Pearson, Albin O.: Characteristics of the Langley 8-Foot Transonic Tunnel With Slotted Test Section. NACA Rep. 1389, 1958. (Supersedes NACA RM L51H10 by Wright and Ritchie and NACA RM L51K14 by Ritchie and Pearson.)

L
1
1
5
0

SECRET

CONFIDENTIAL

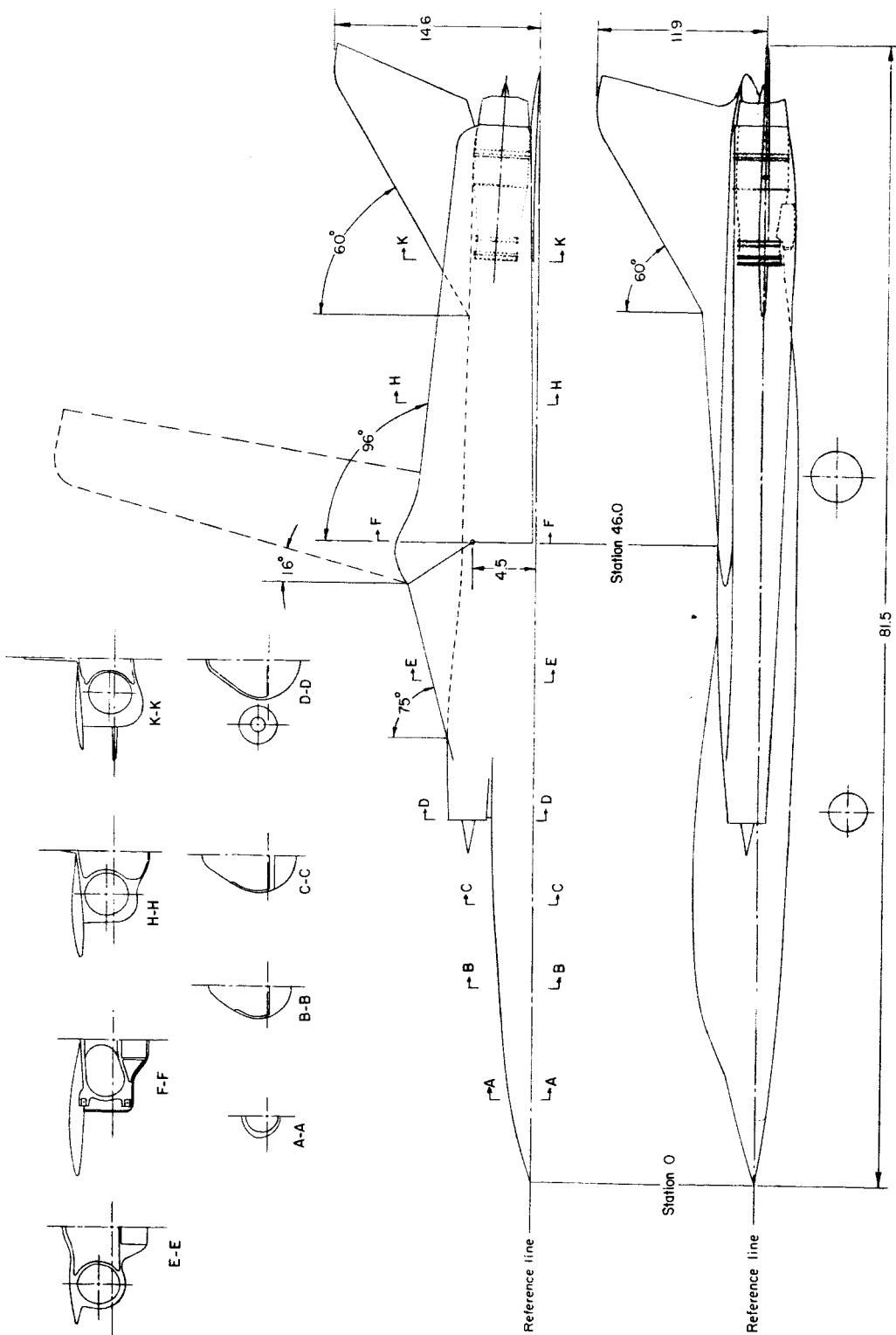


Figure 1.- General arrangement of configuration VII. All dimensions in feet unless otherwise noted.

CONFIDENTIAL

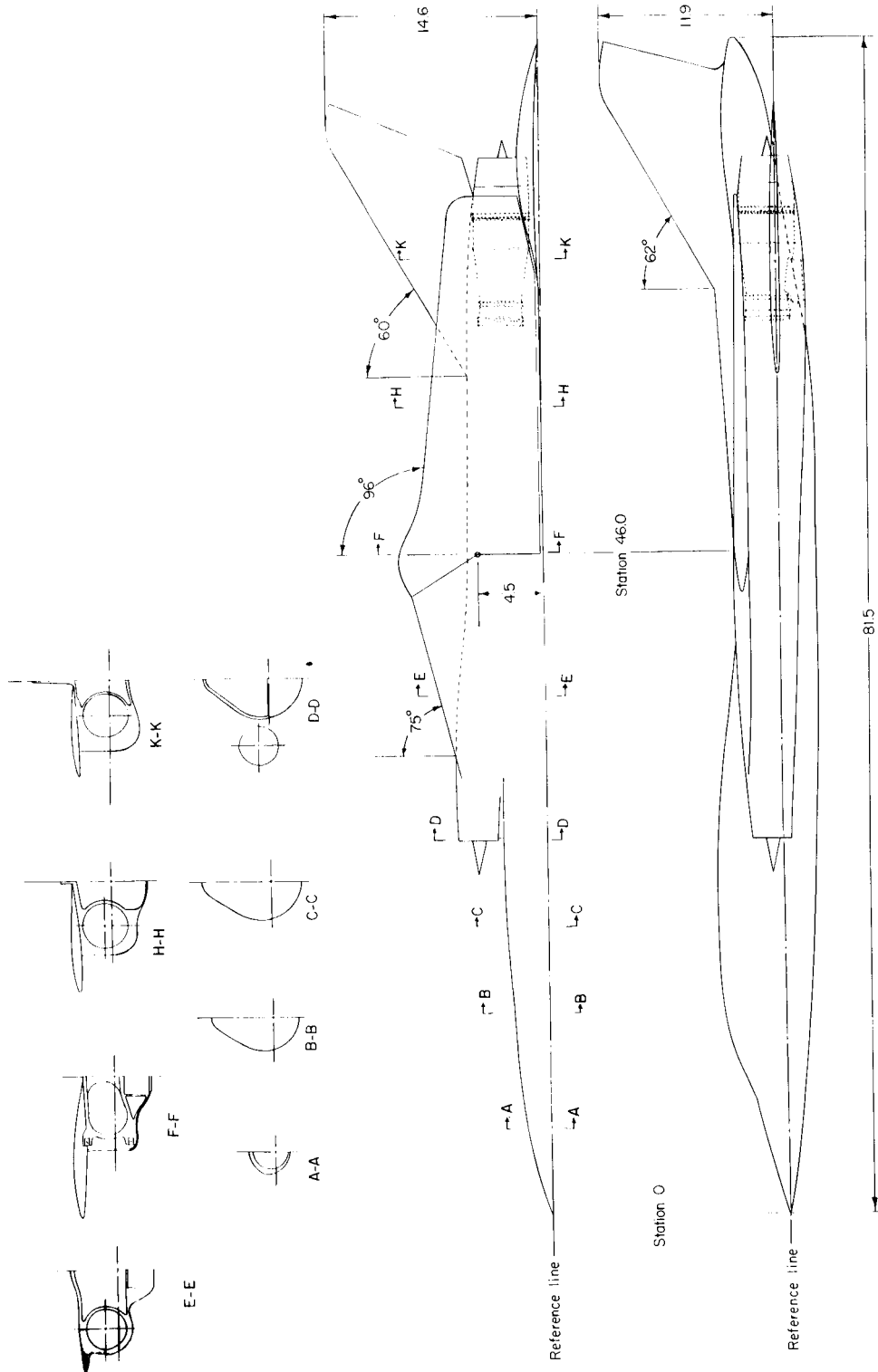


Figure 2.- General arrangement of configuration VIIA. All dimensions in feet unless otherwise noted.

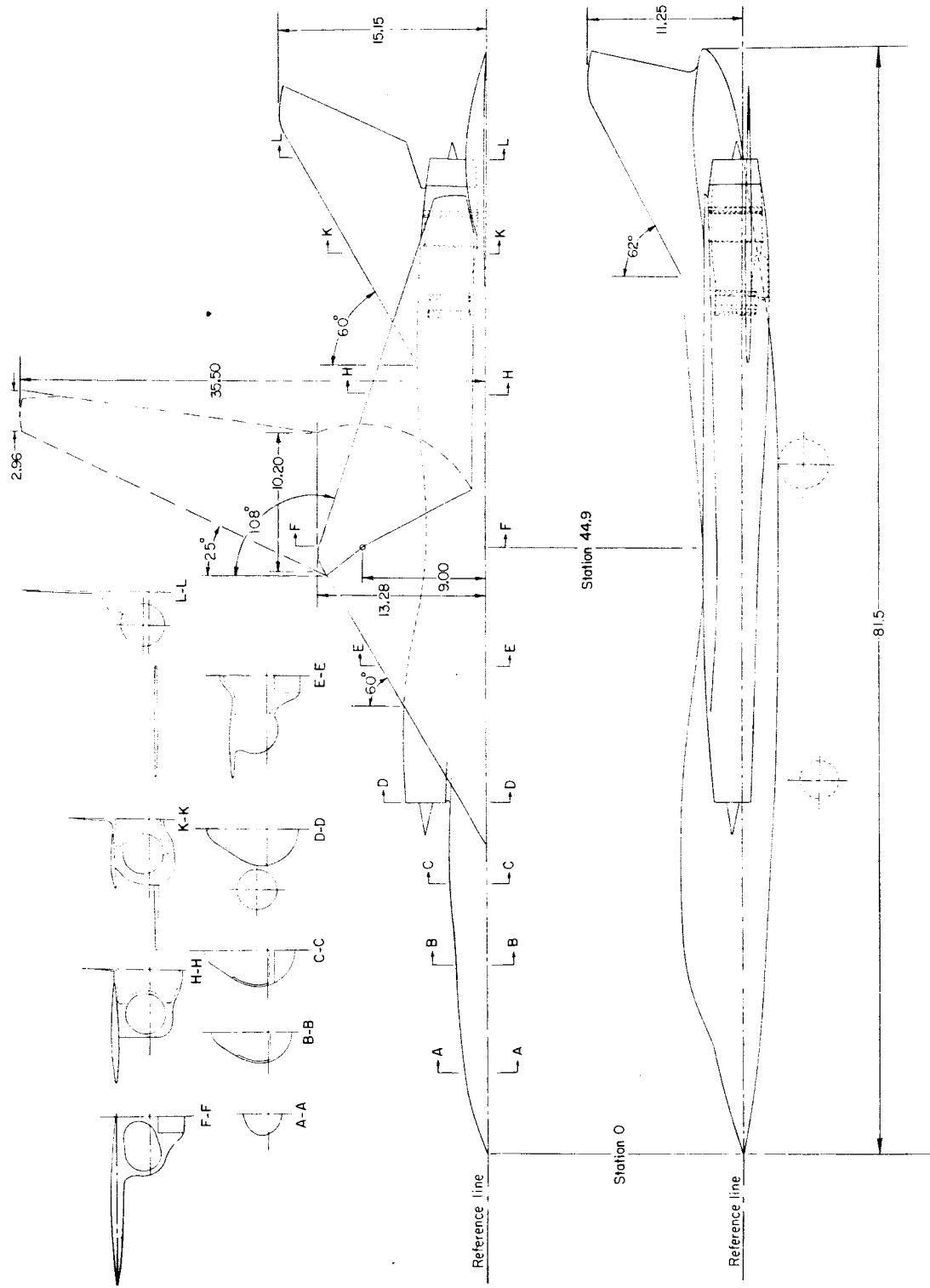


Figure 3.- General arrangement of configuration VIII. All dimensions in feet unless otherwise noted.

CONFIDENTIAL

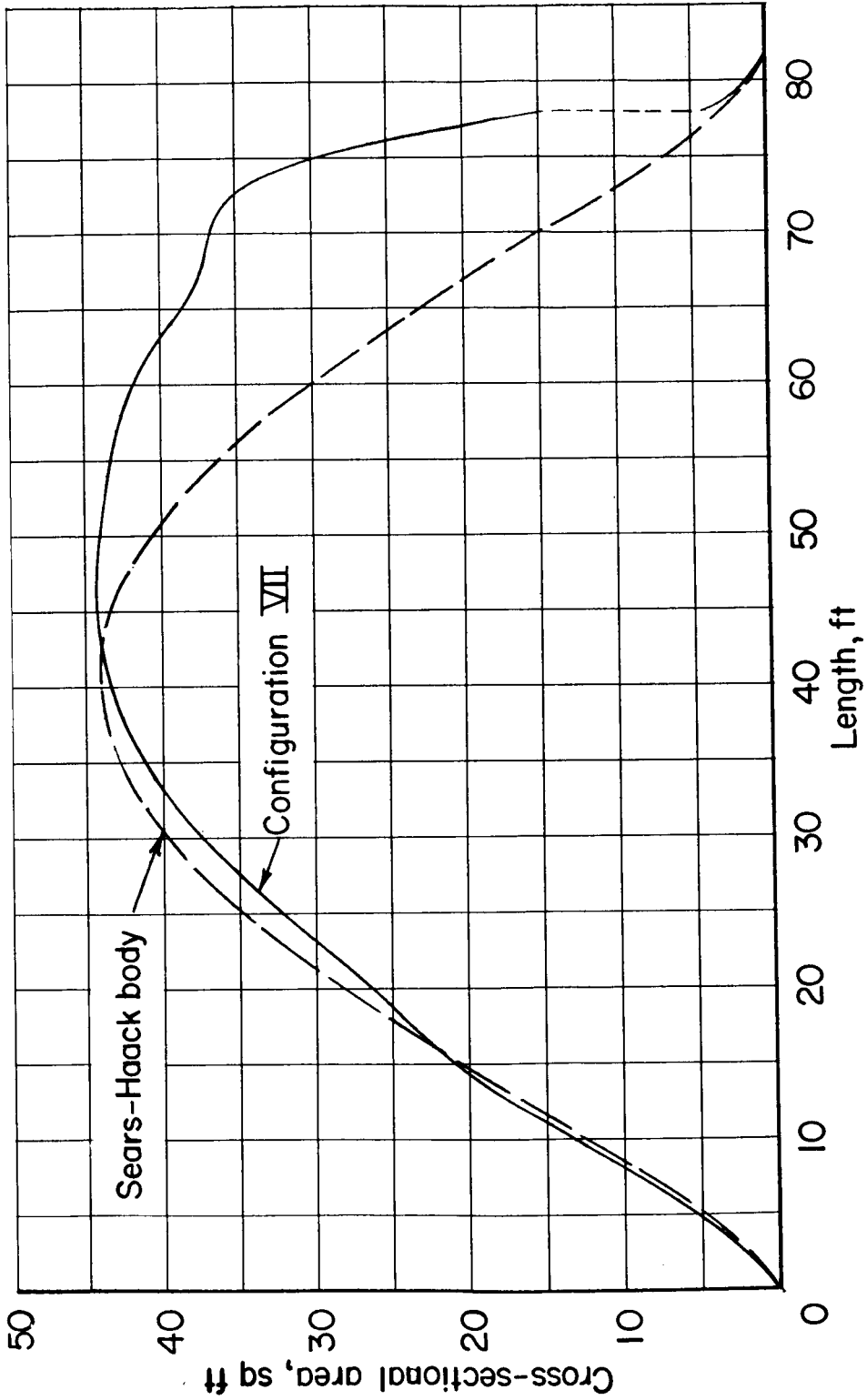


Figure 4.- Cross-sectional-area curves of configuration VII.

CONFIDENTIAL

SECRET

L-1150

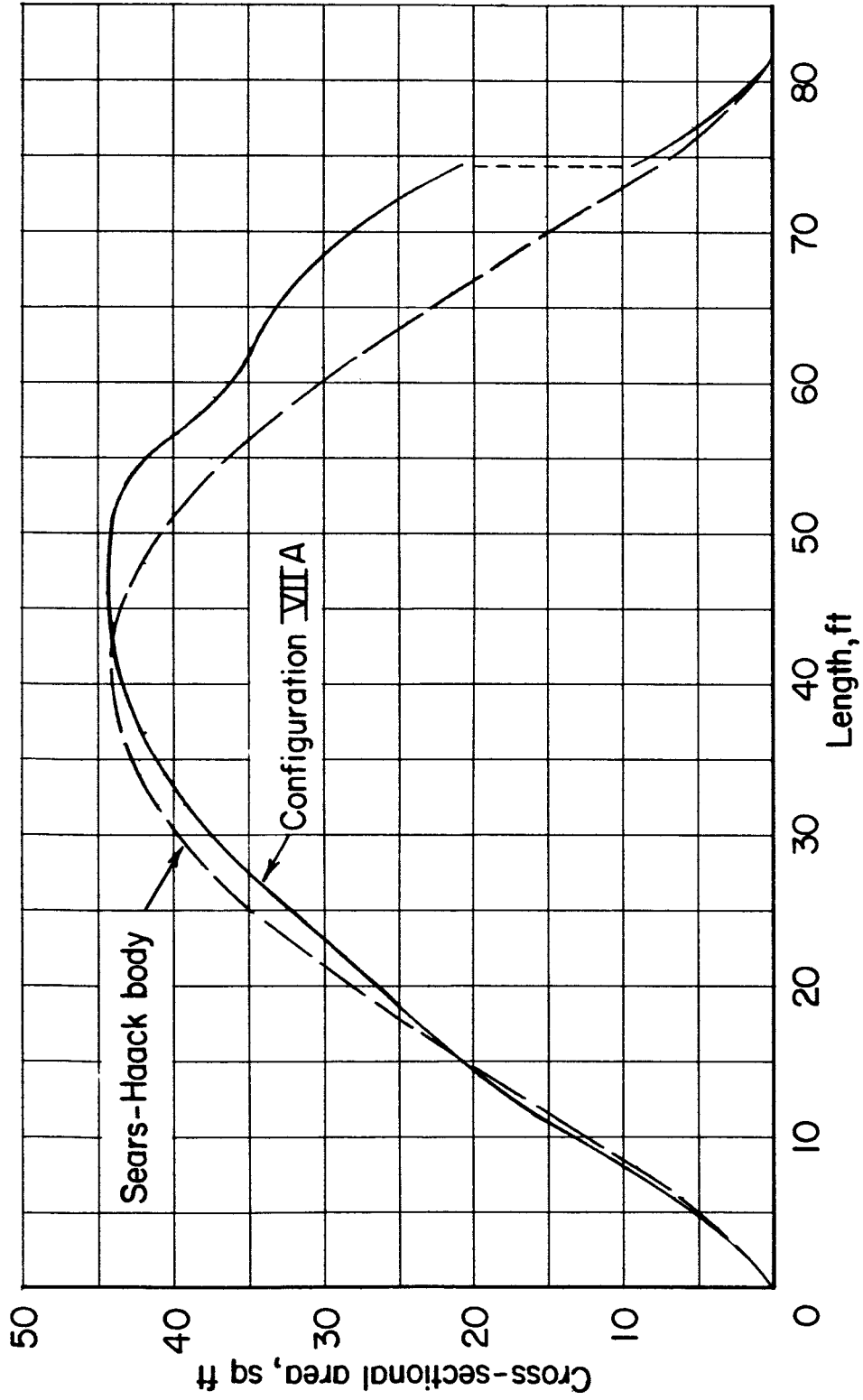


Figure 5.- Cross-sectional-area curves of configuration VIIA.

CONFIDENTIAL

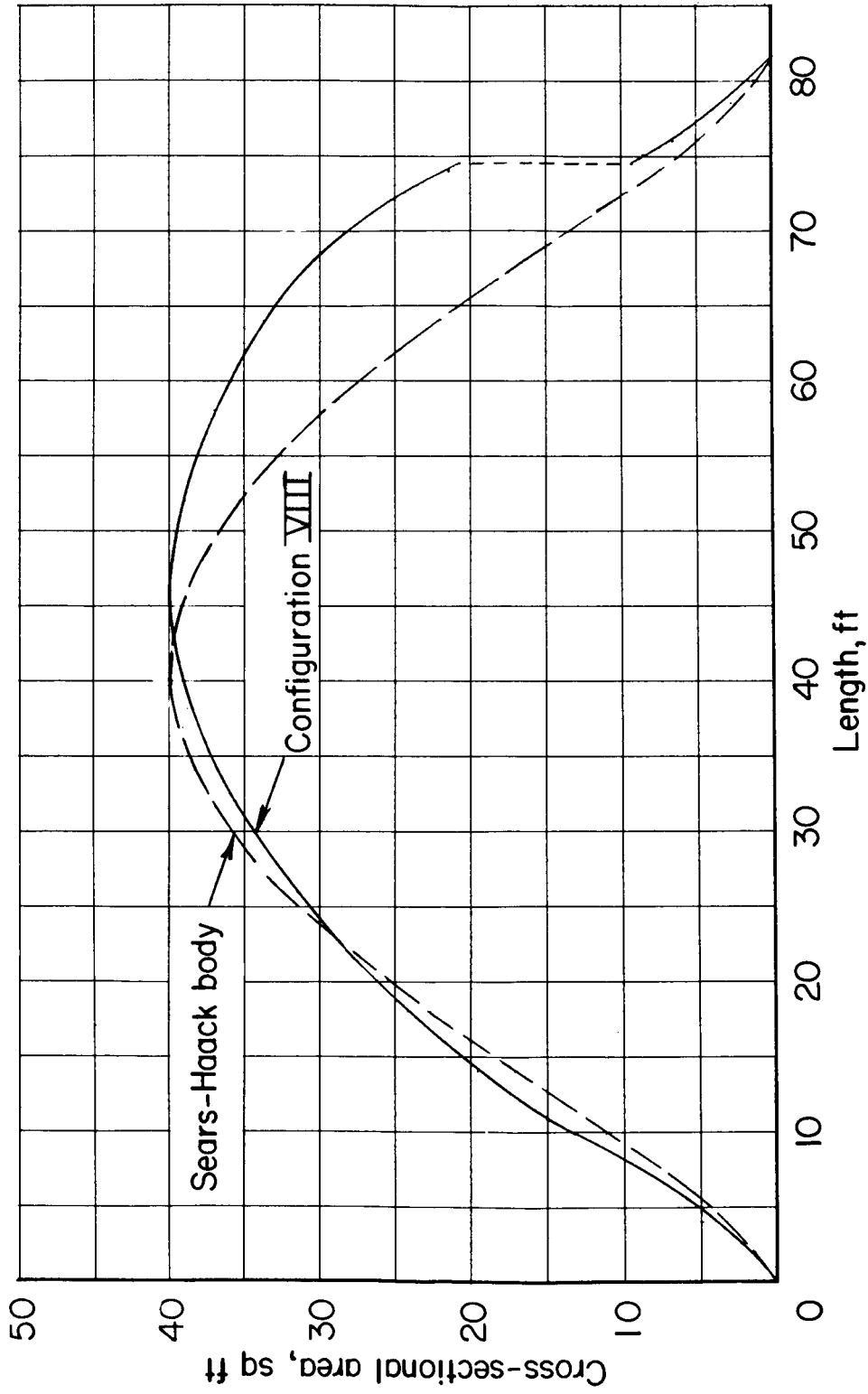
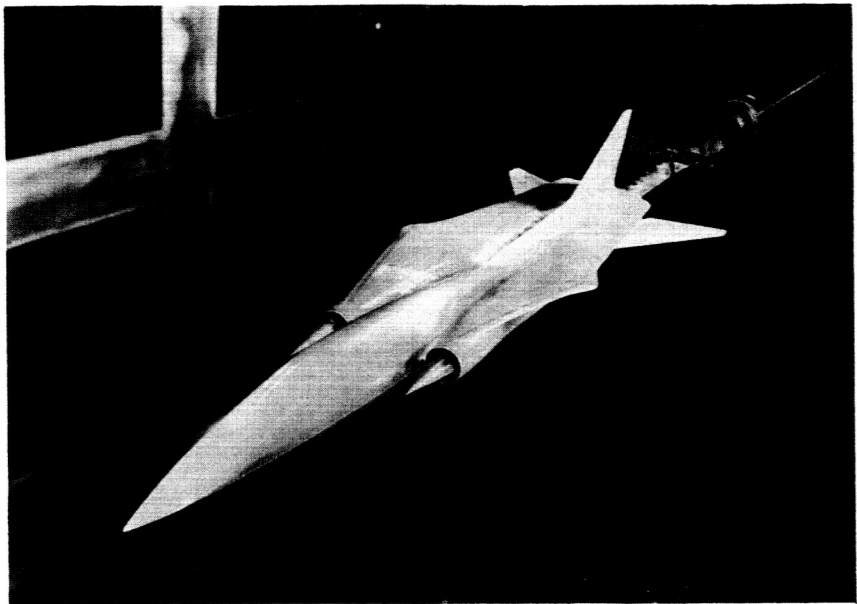
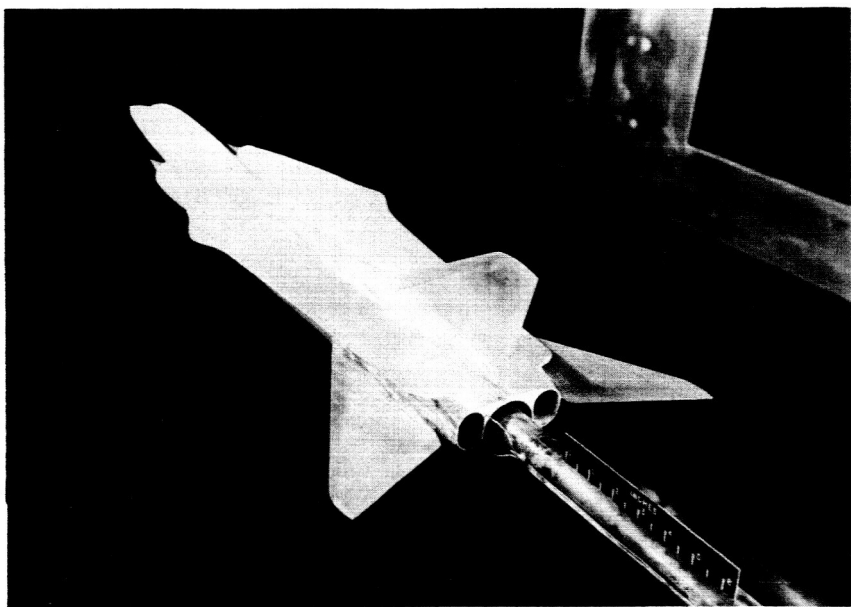


Figure 6.- Cross-sectional-area curves of configuration VIII.

L-1150

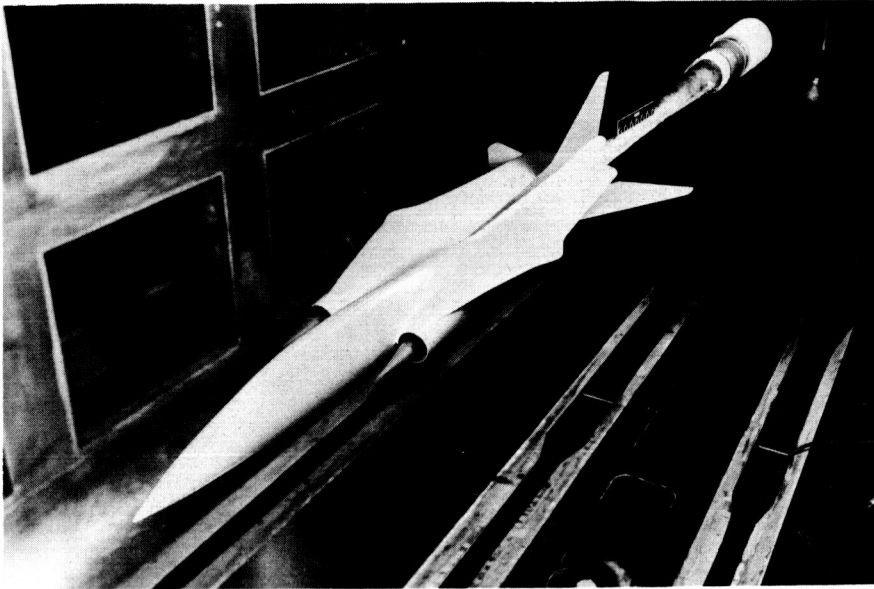


(a) Three-quarter front view. L-60-1950



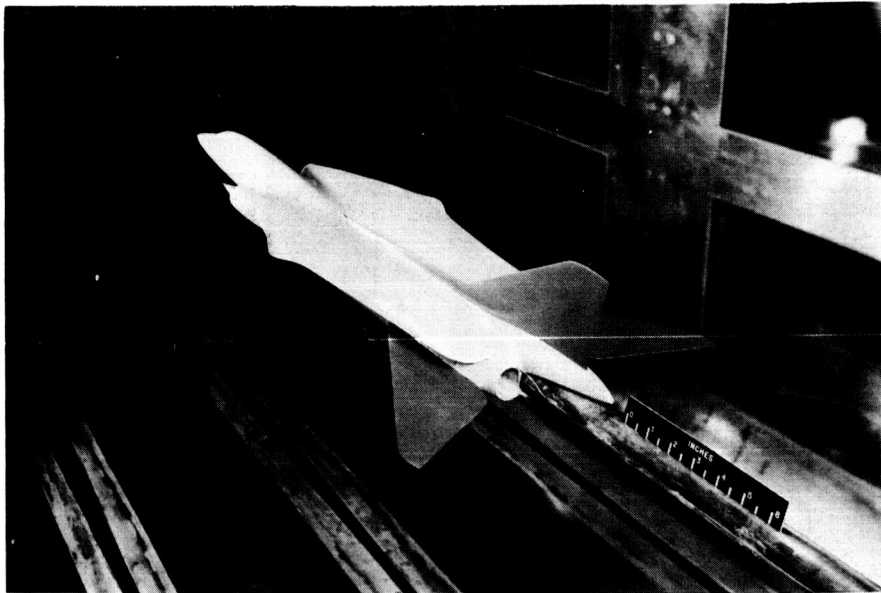
(b) Three-quarter rear view. L-60-1951

Figure 7.- Configuration VII tested in Langley 8-foot transonic pressure tunnel.



(a) Three-quarter front view.

L-60-1952



(b) Three-quarter rear view.

L-60-1953

Figure 8.- Configuration VIIA tested in Langley 8-foot transonic pressure tunnel.

L-1150



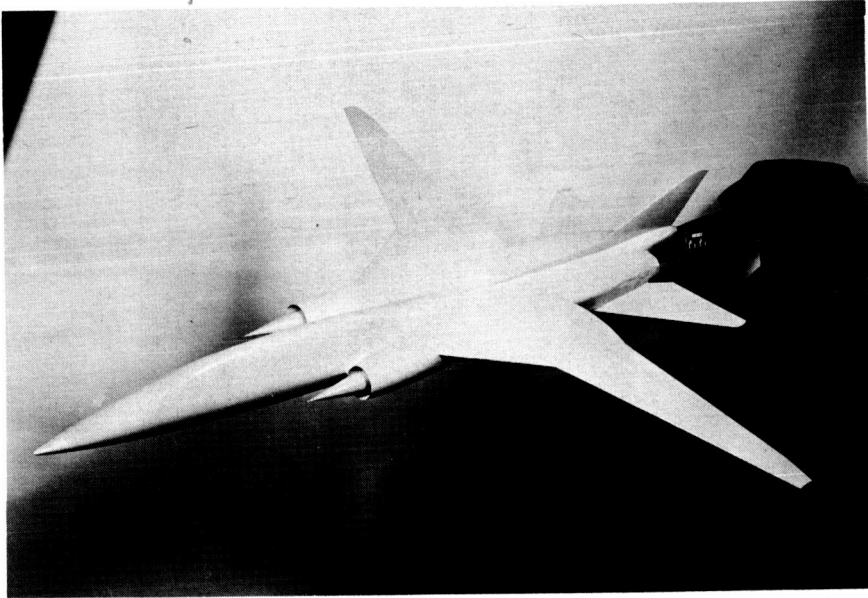
CONFIDENTIAL



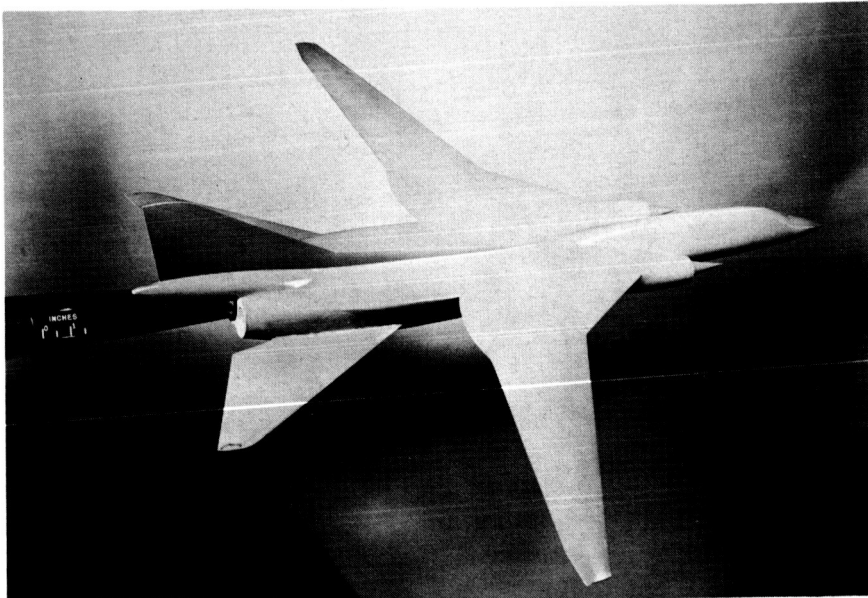
L-60-2015
Figure 9.- Configuration VIIA with reconnaissance pod tested in Langley
8-foot transonic pressure tunnel.

L-1150

037 [REDACTED] 034



(a) Three-quarter front view. L-60-2014



(b) Three-quarter rear view. L-60-2013

Figure 10.- Configuration VIII with wing swept back 25° tested in Langley 8-foot transonic pressure tunnel.

[REDACTED]

I-1150

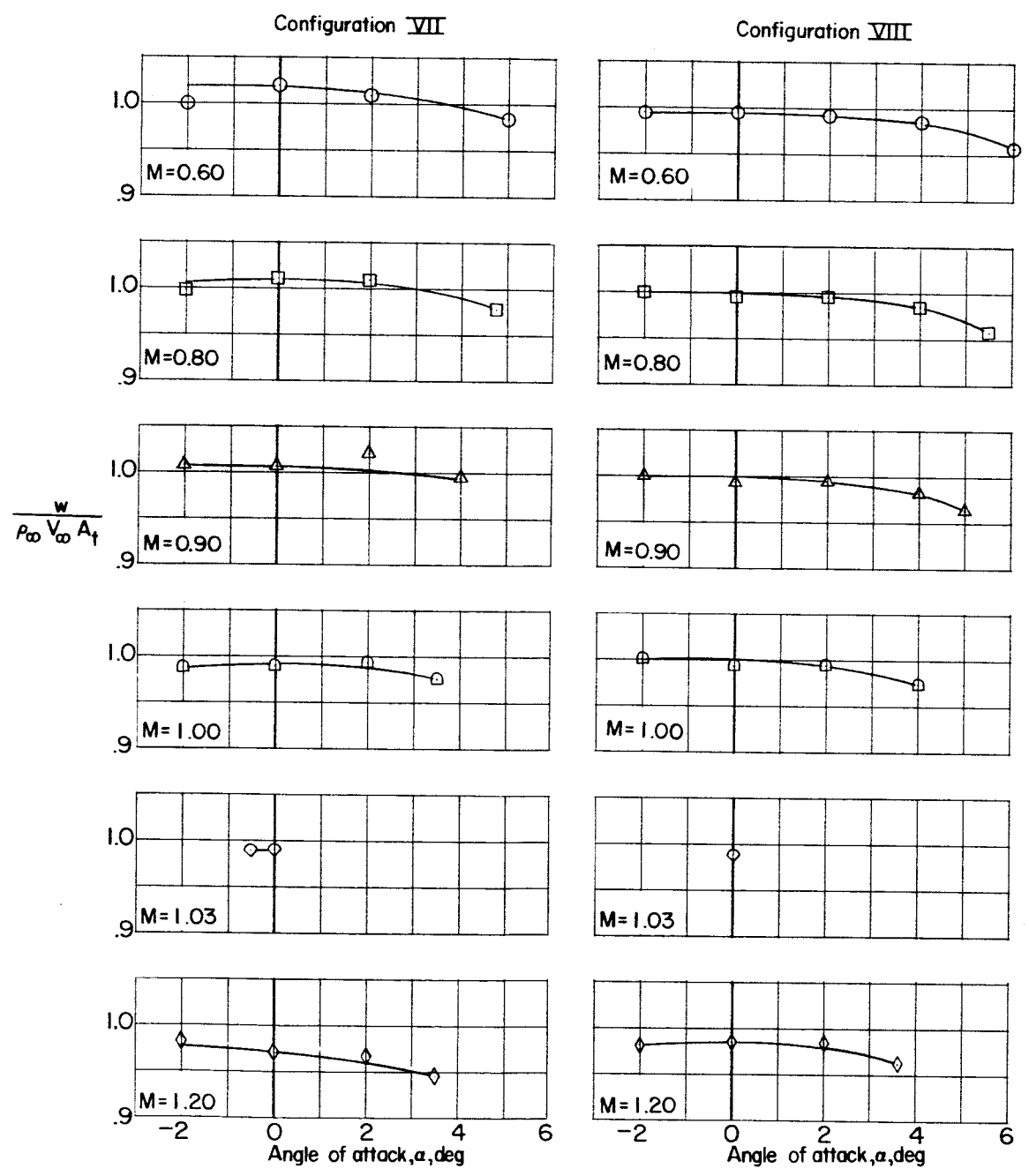


Figure 11.- Variation of mass-flow ratio with angle of attack for configurations VII and VIII. ($A_t = 0.00742$ square foot per duct, model scale.)

CONFIDENTIAL

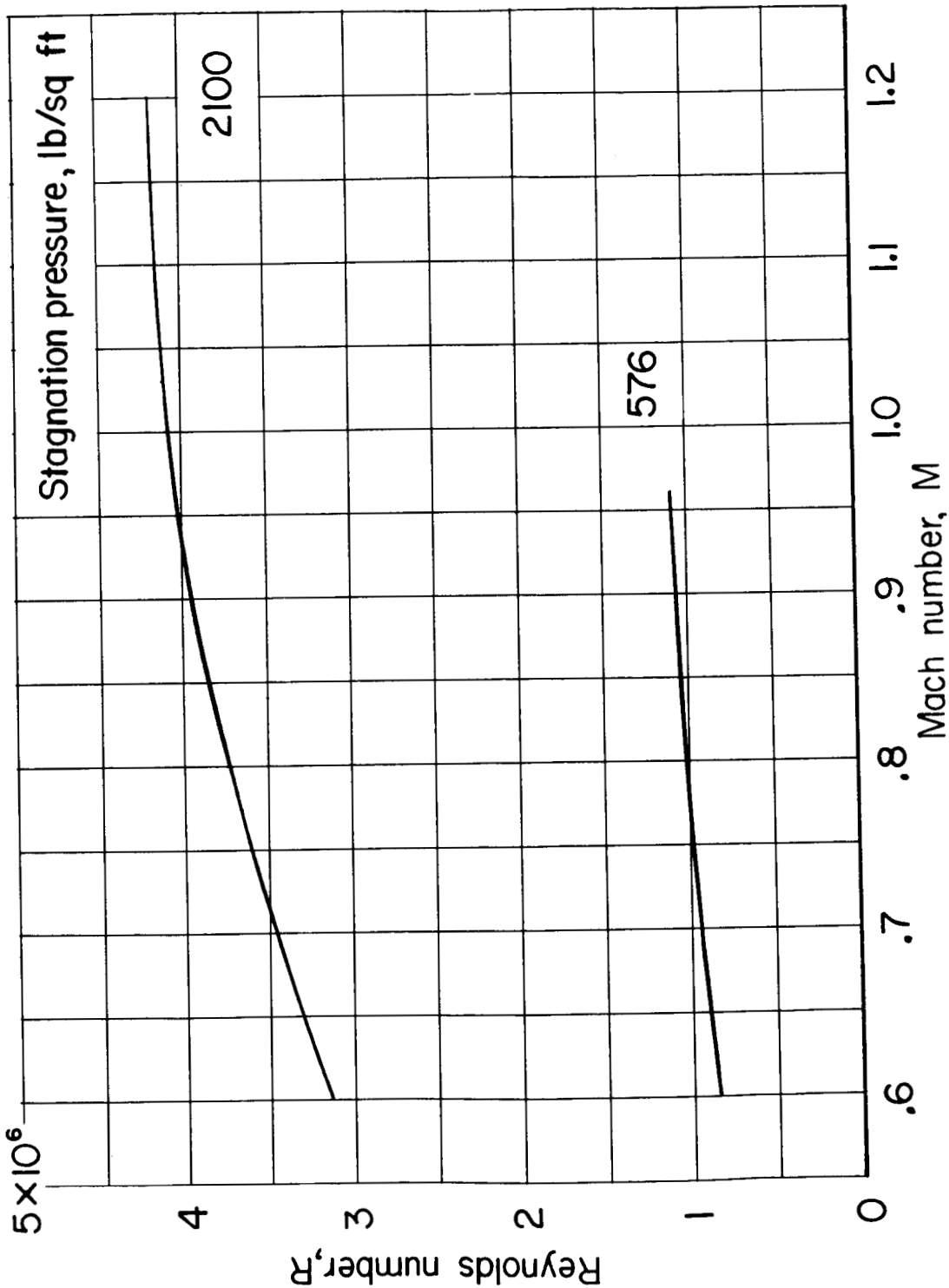
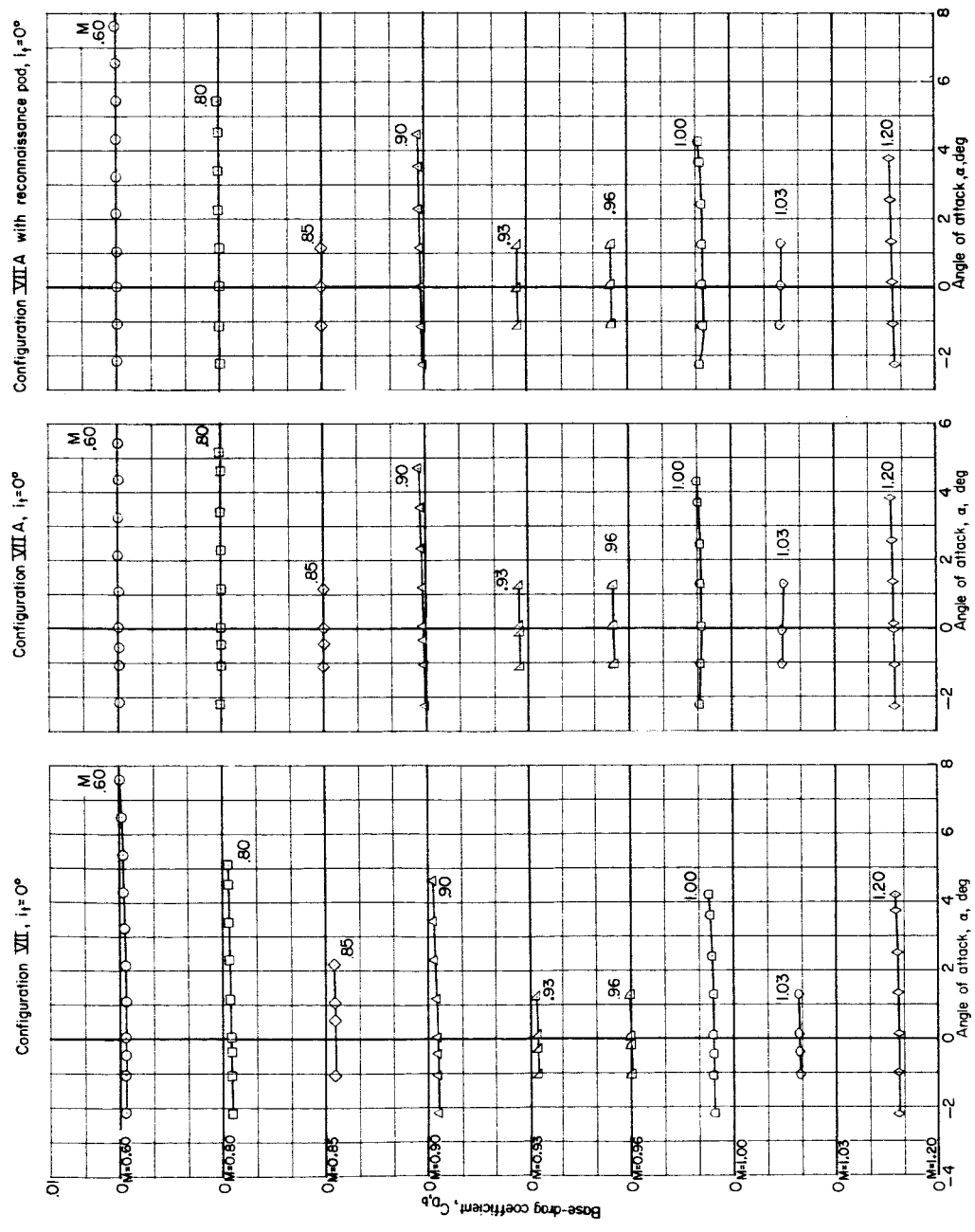


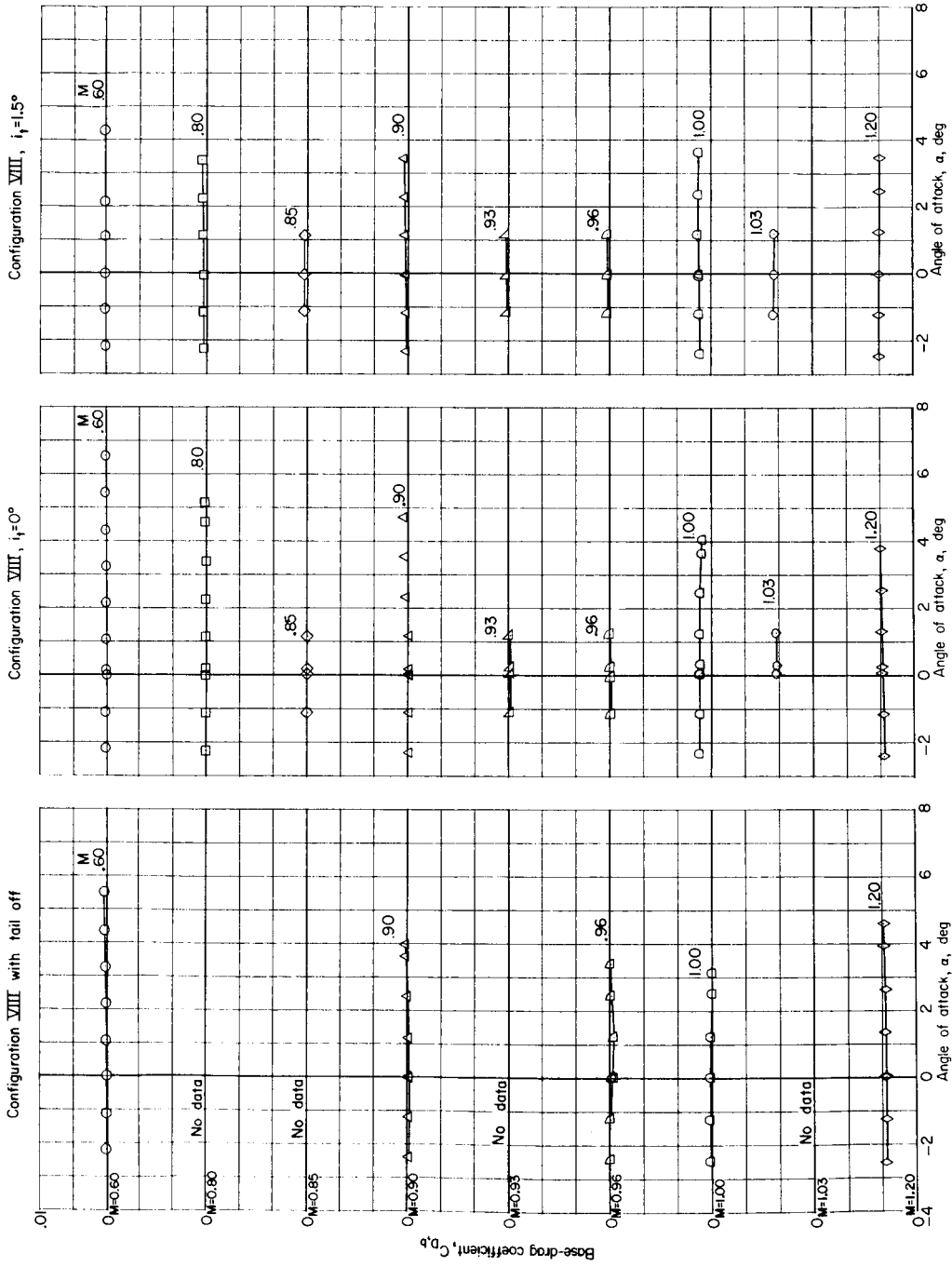
Figure 12.- Variation with Mach number of test Reynolds number based on reference chord of 1 foot.

SECRET



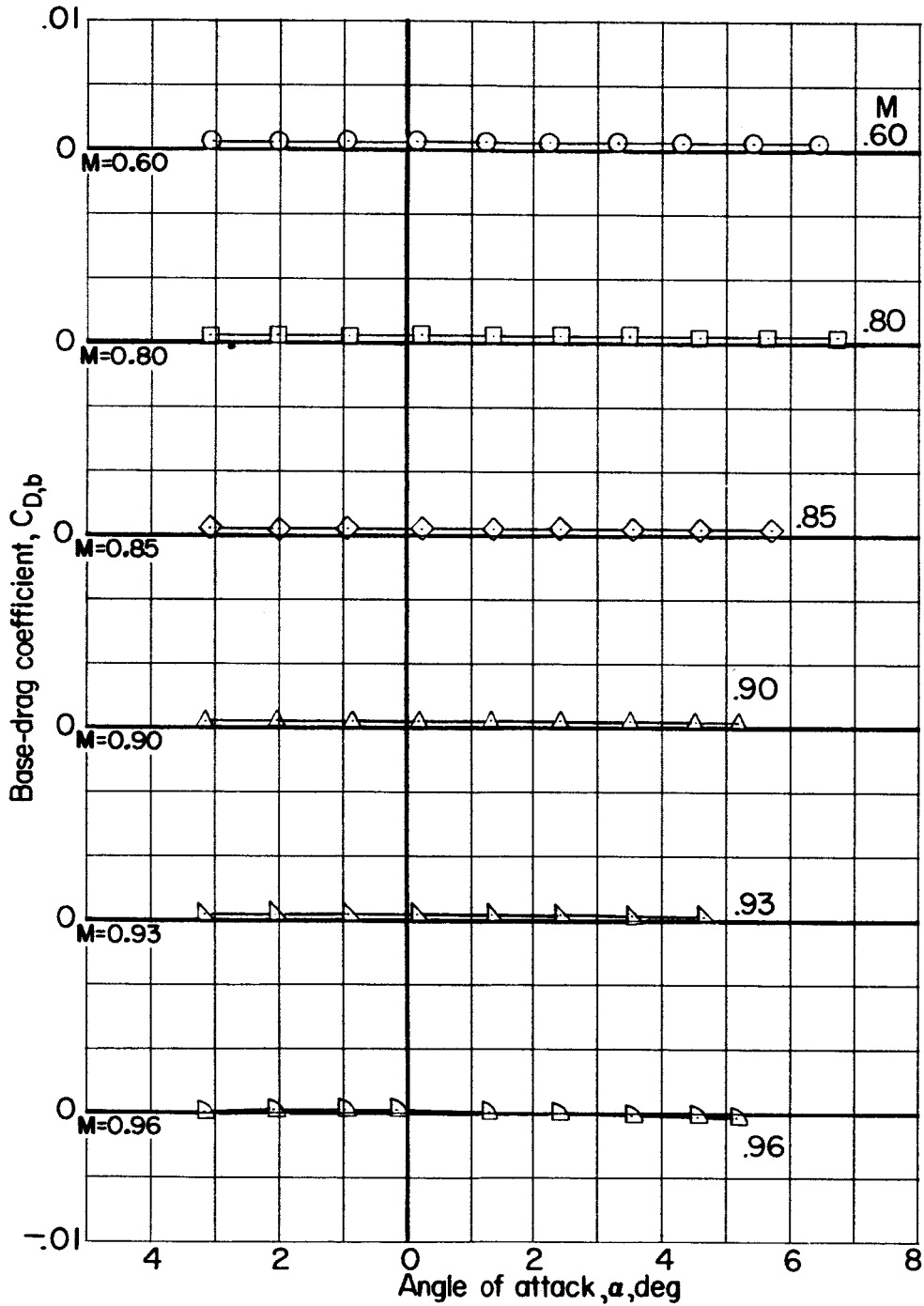
(a) Configurations VII and VIIA.

Figure 13.- Variation of base-drag coefficients with angle of attack for configurations tested.



(b) Configuration VIII.

Figure 13.- Continued.



(c) Configuration VIII with wing swept back 25° .

Figure 13.- Concluded.

L-1150

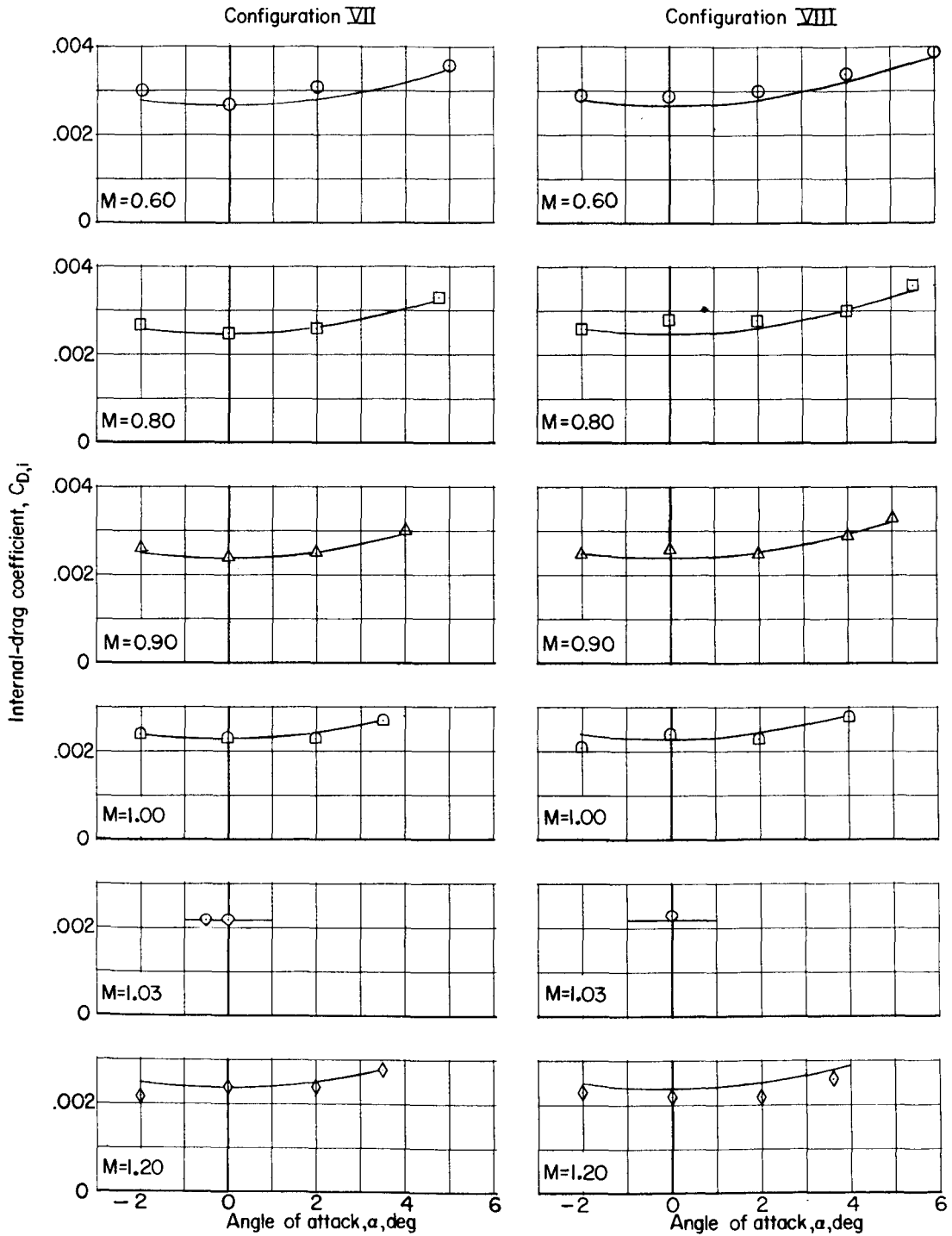
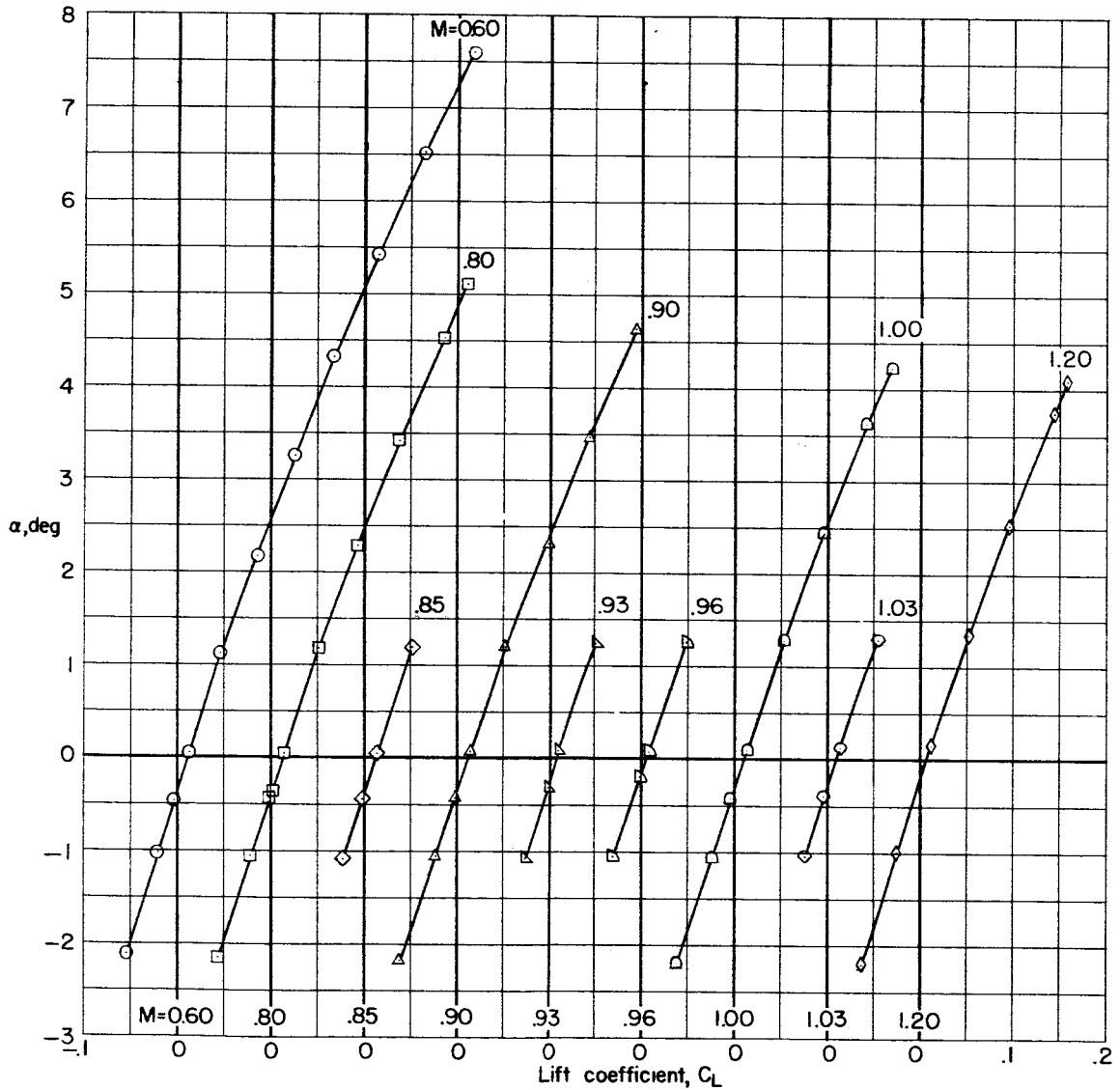


Figure 14.- Variation of internal-drag coefficient with angle of attack for configurations VII and VIII.

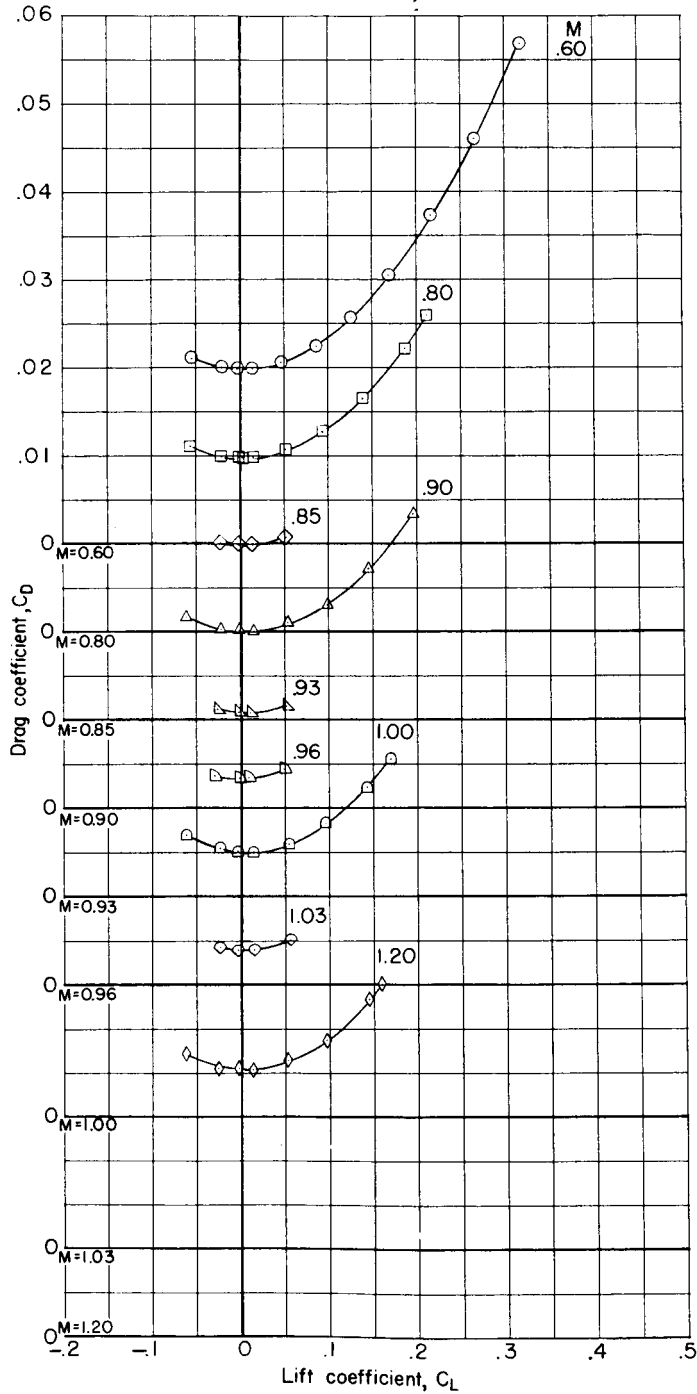
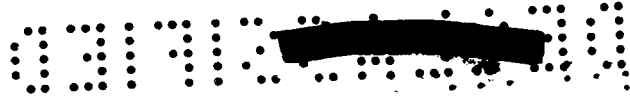


L-1150



(a) Angle of attack.

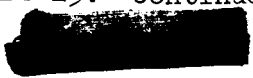
Figure 15.- Aerodynamic characteristics of configuration VII.
 $i_t = 0^\circ$.

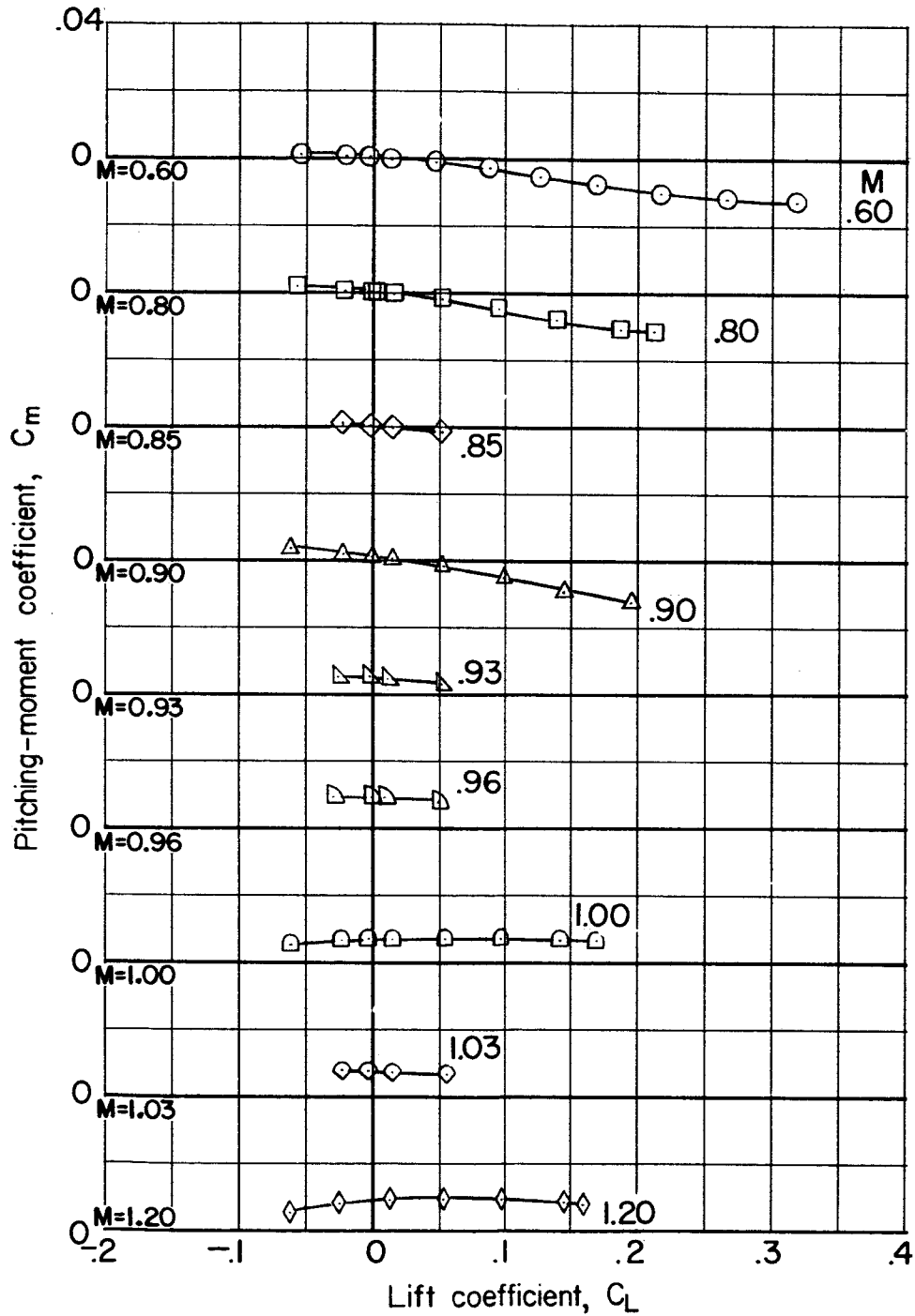


L-1150

(b) Drag coefficient.

Figure 15.- Continued.



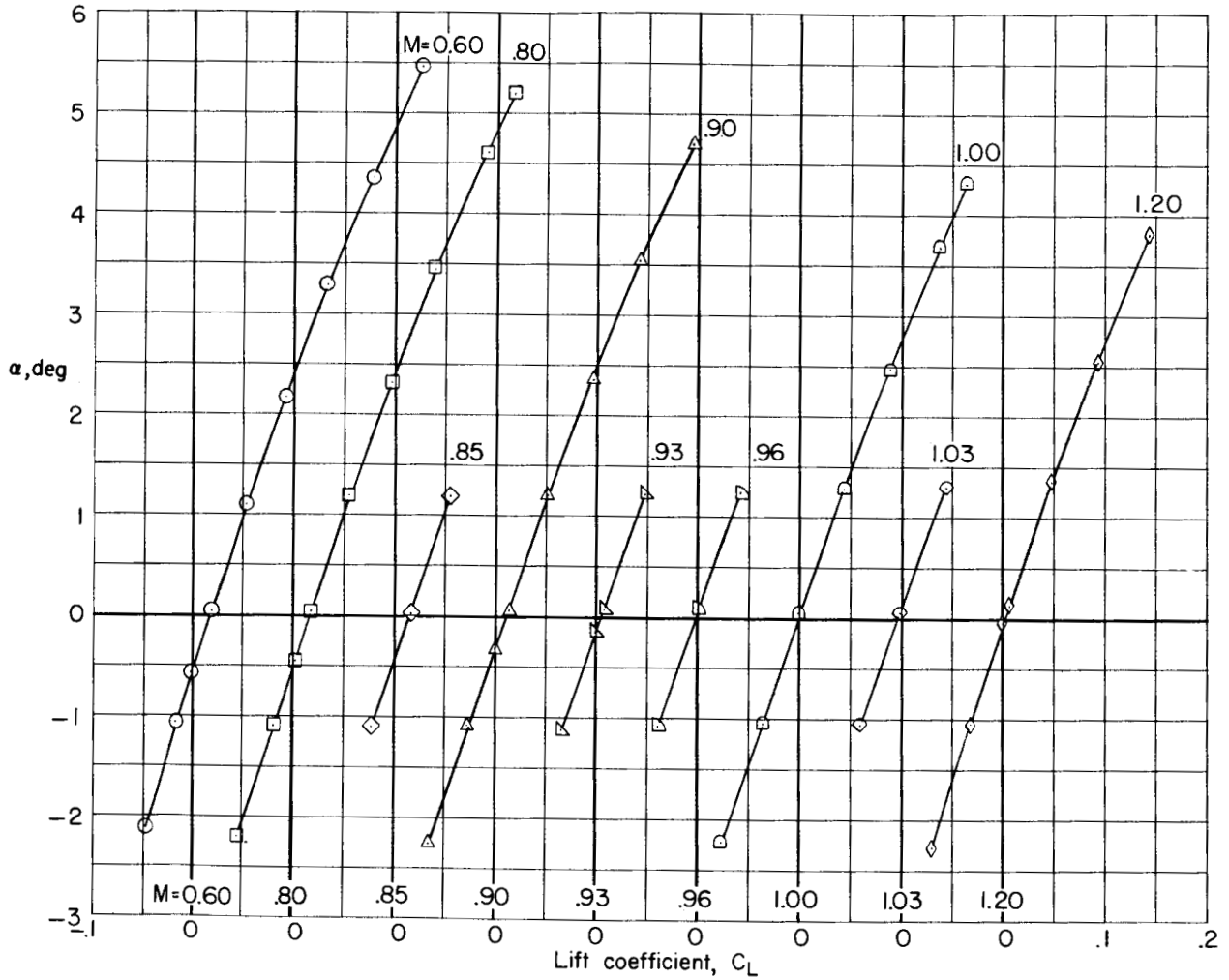


(c) Pitching-moment coefficient.

Figure 15.- Concluded.



L-1150

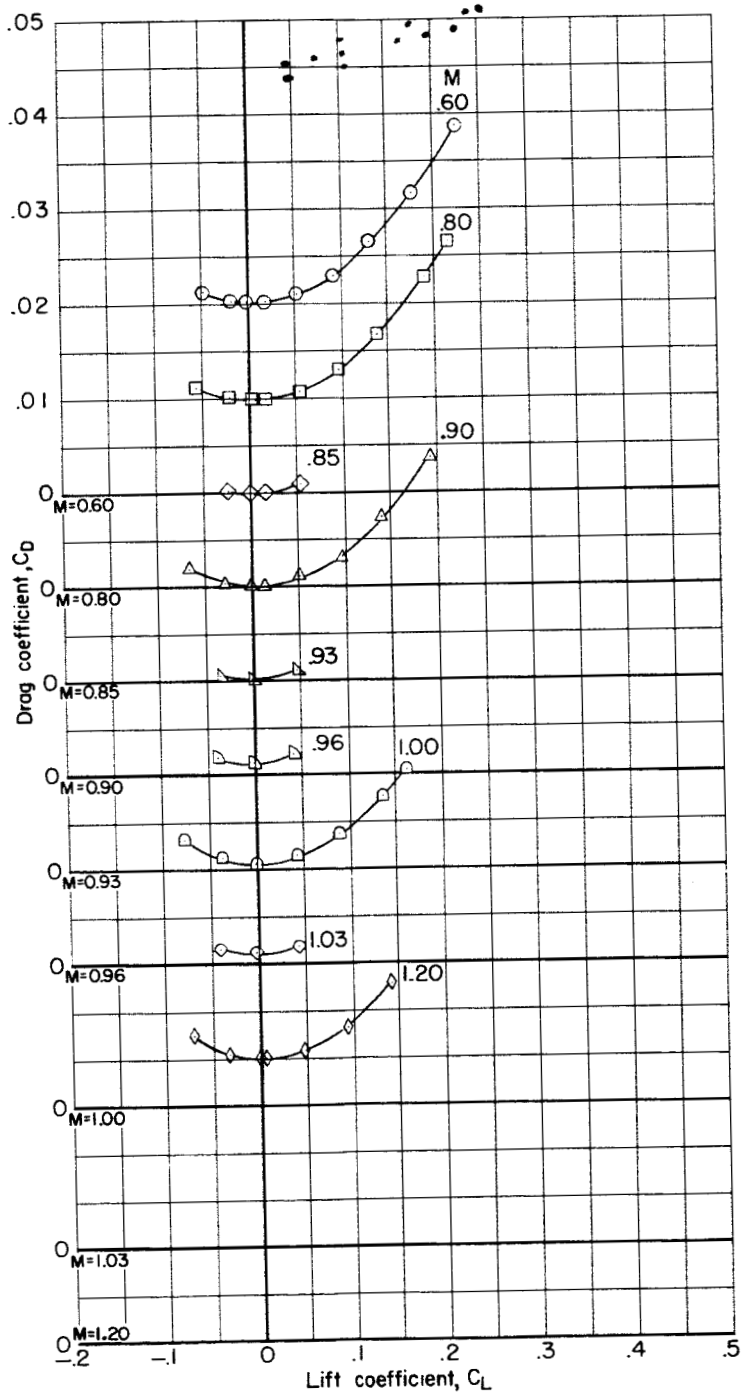


(a) Angle of attack.

Figure 16.- Aerodynamic characteristics of configuration VIIA. $i_t = 0^\circ$.



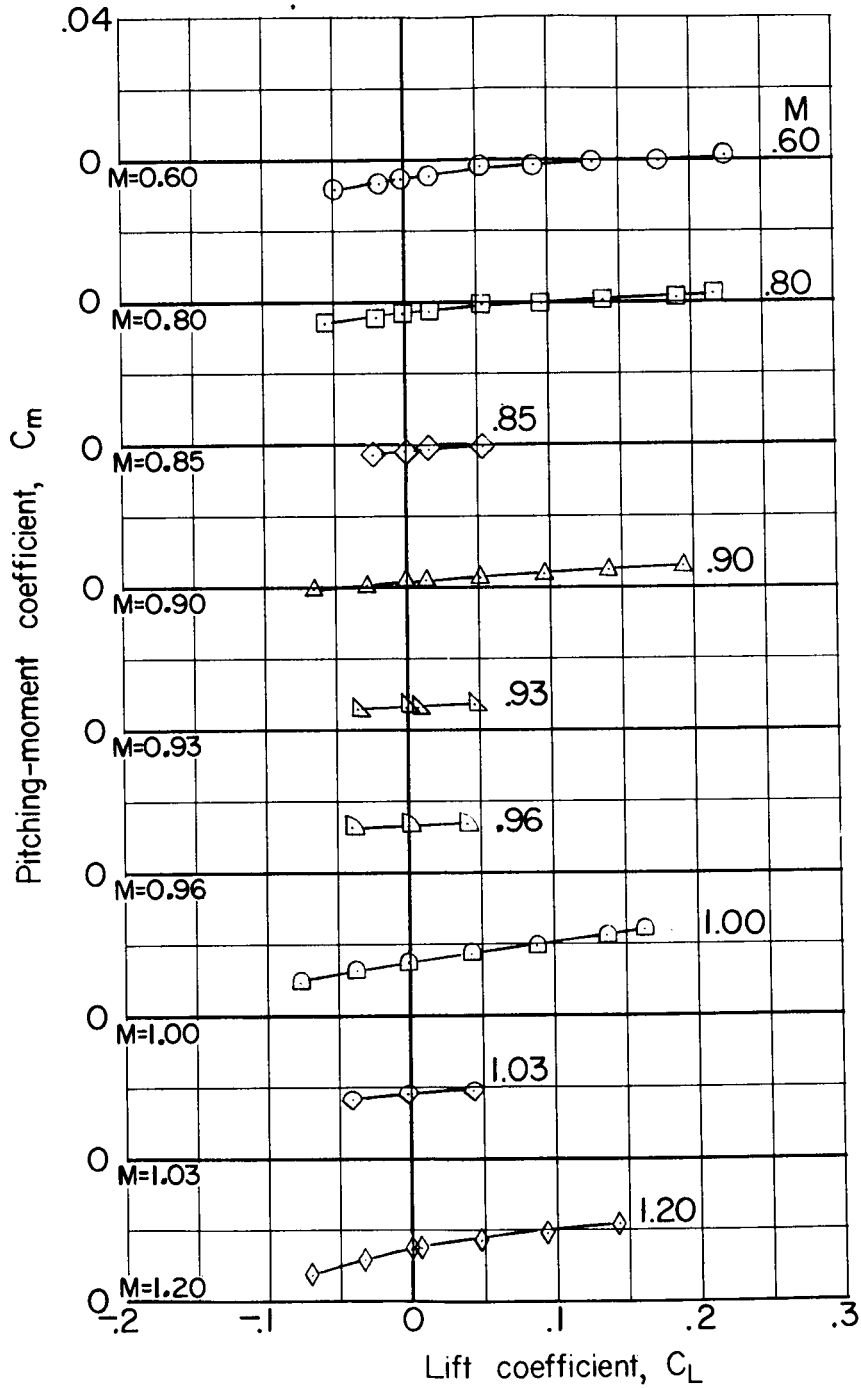
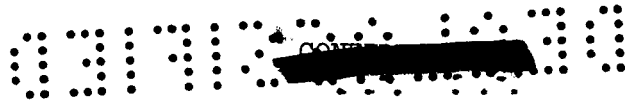
L-1150



(b) Drag coefficient.

Figure 16.- Continued.



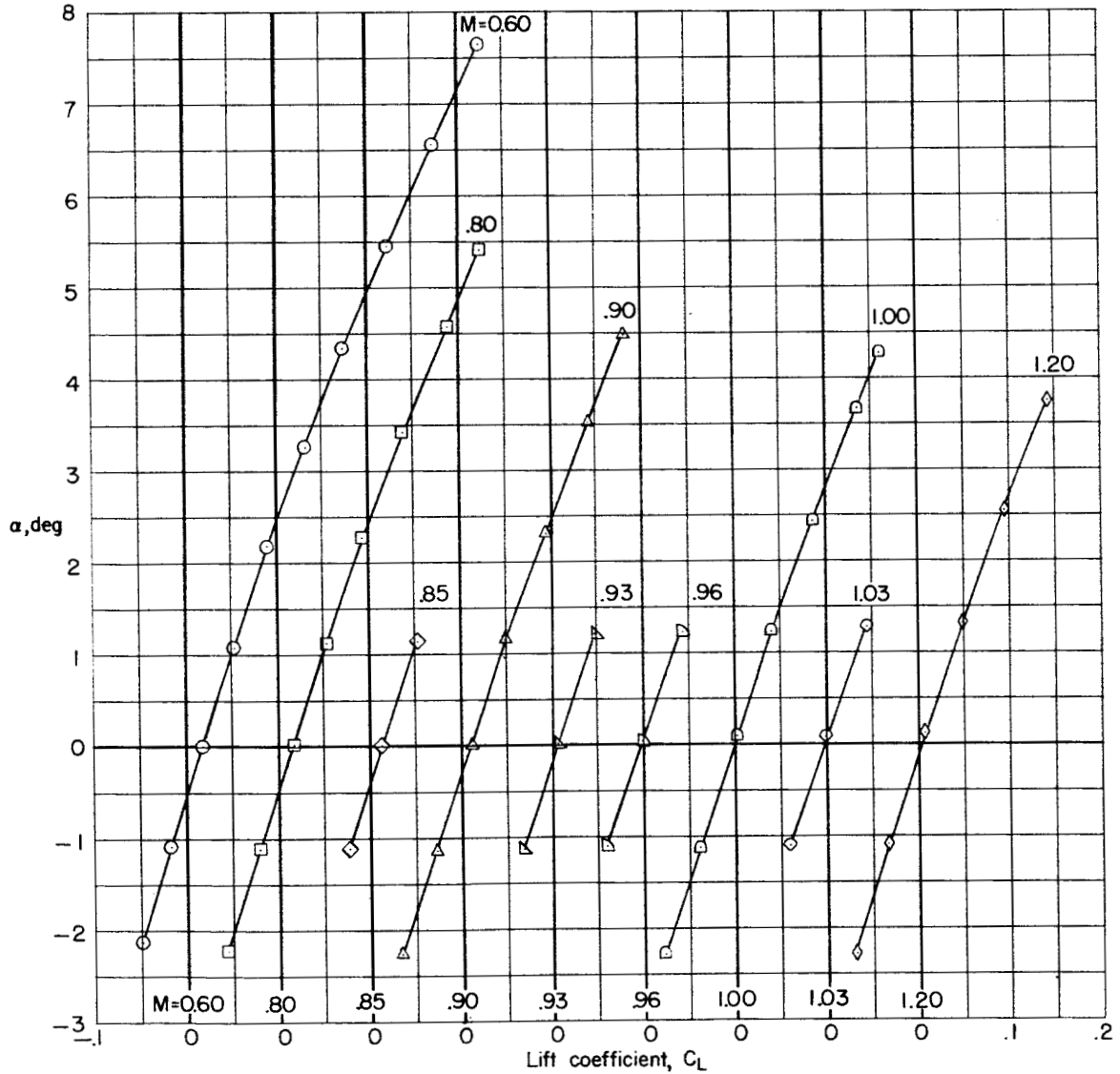


(c) Pitching-moment coefficient.

Figure 16.- Concluded.



L-1150

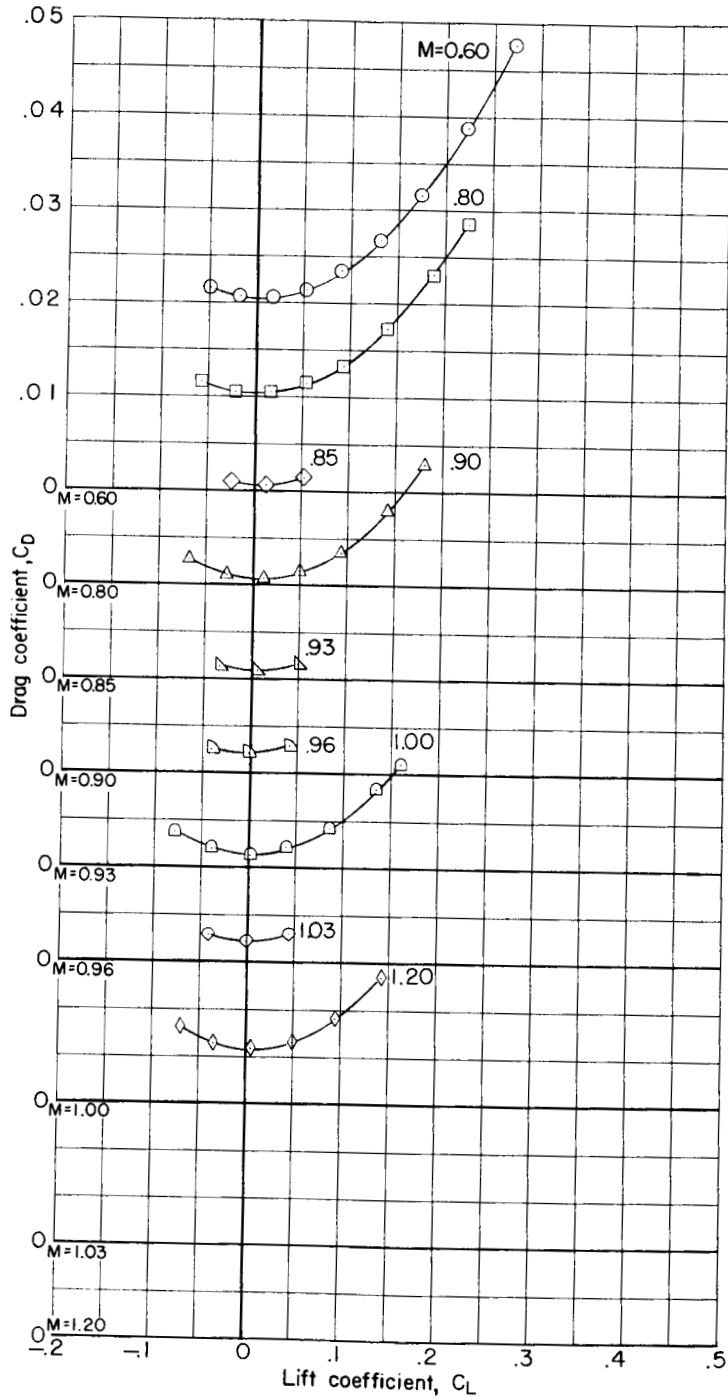


(a) Angle of attack.

Figure 17.- Aerodynamic characteristics of configuration VIIA with reconnaissance pod. $i_t = 0^\circ$.



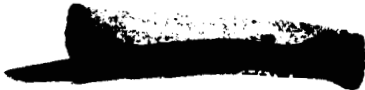
L-1150

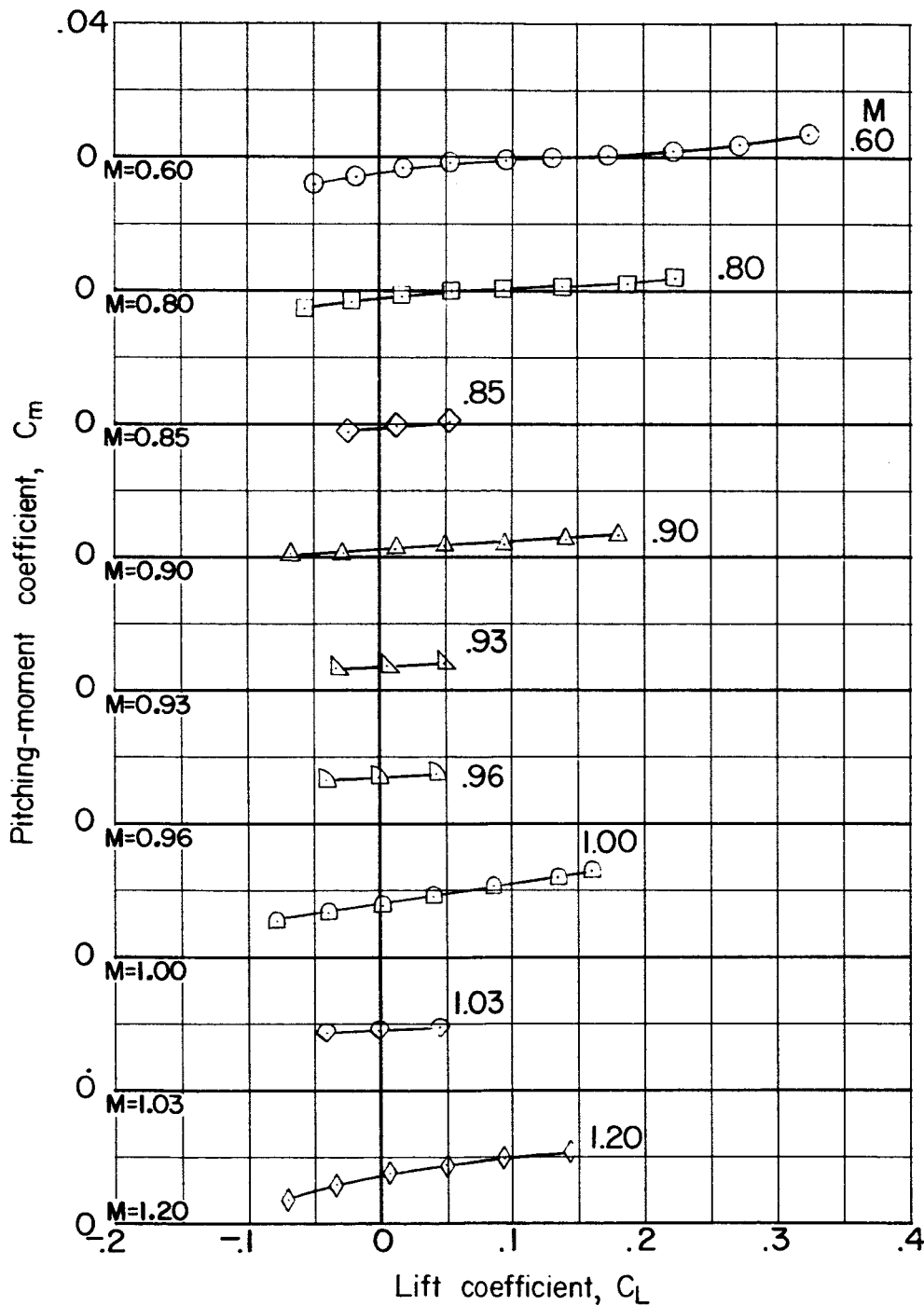


L-1150

(b) Drag coefficient.

Figure 17.- Continued.

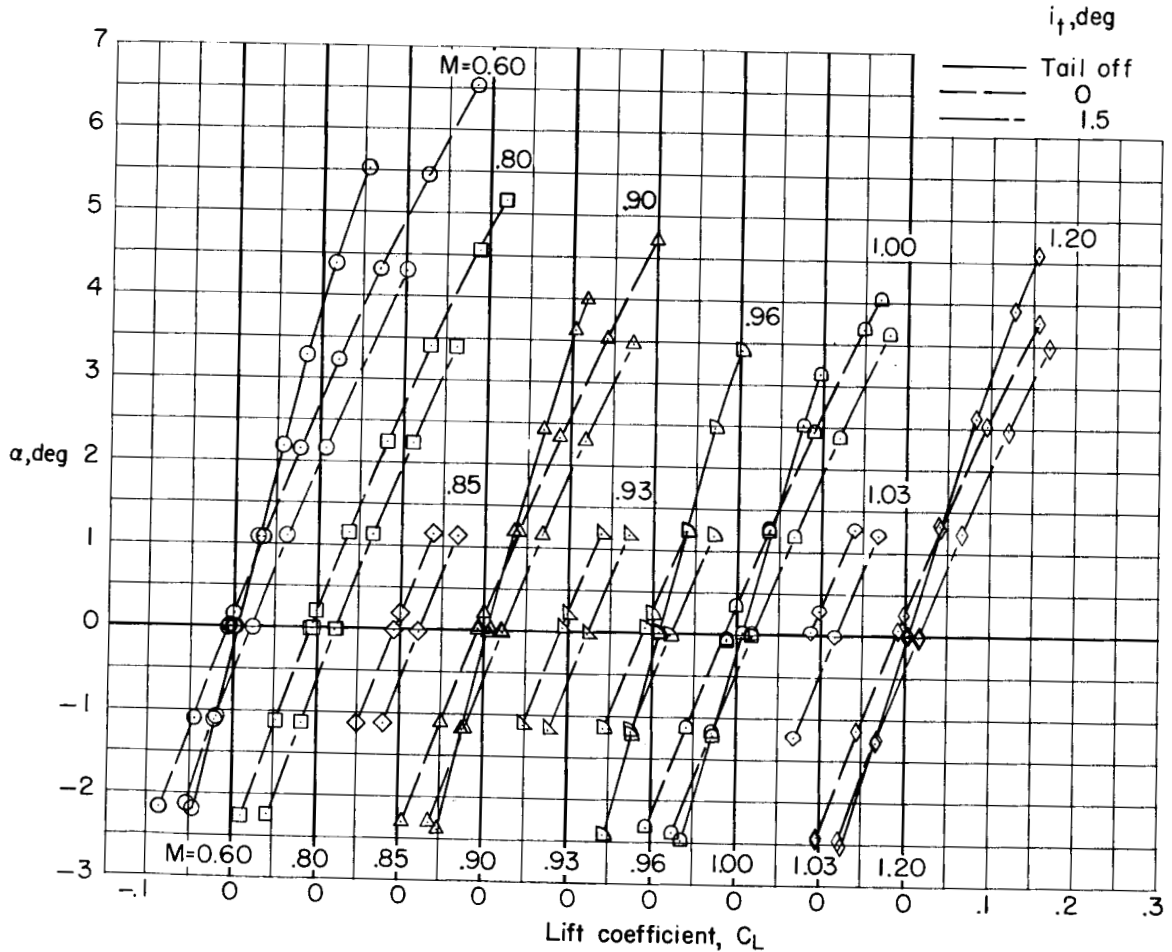
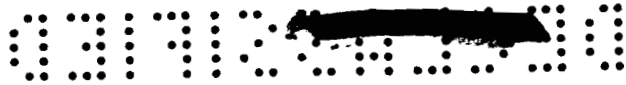




(c) Pitching-moment coefficient.

Figure 17.- Concluded.



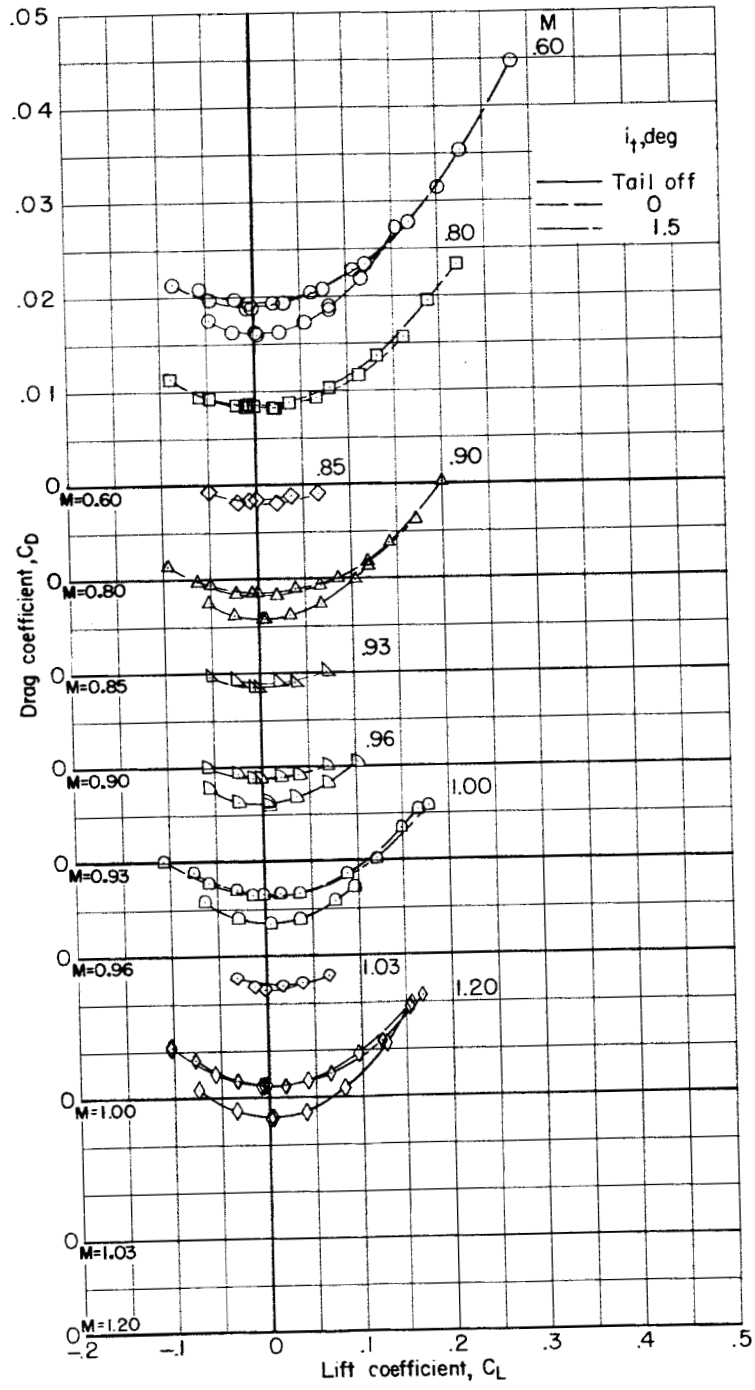


(a) Angle of attack.

Figure 18.- Aerodynamic characteristics of configuration VIII.



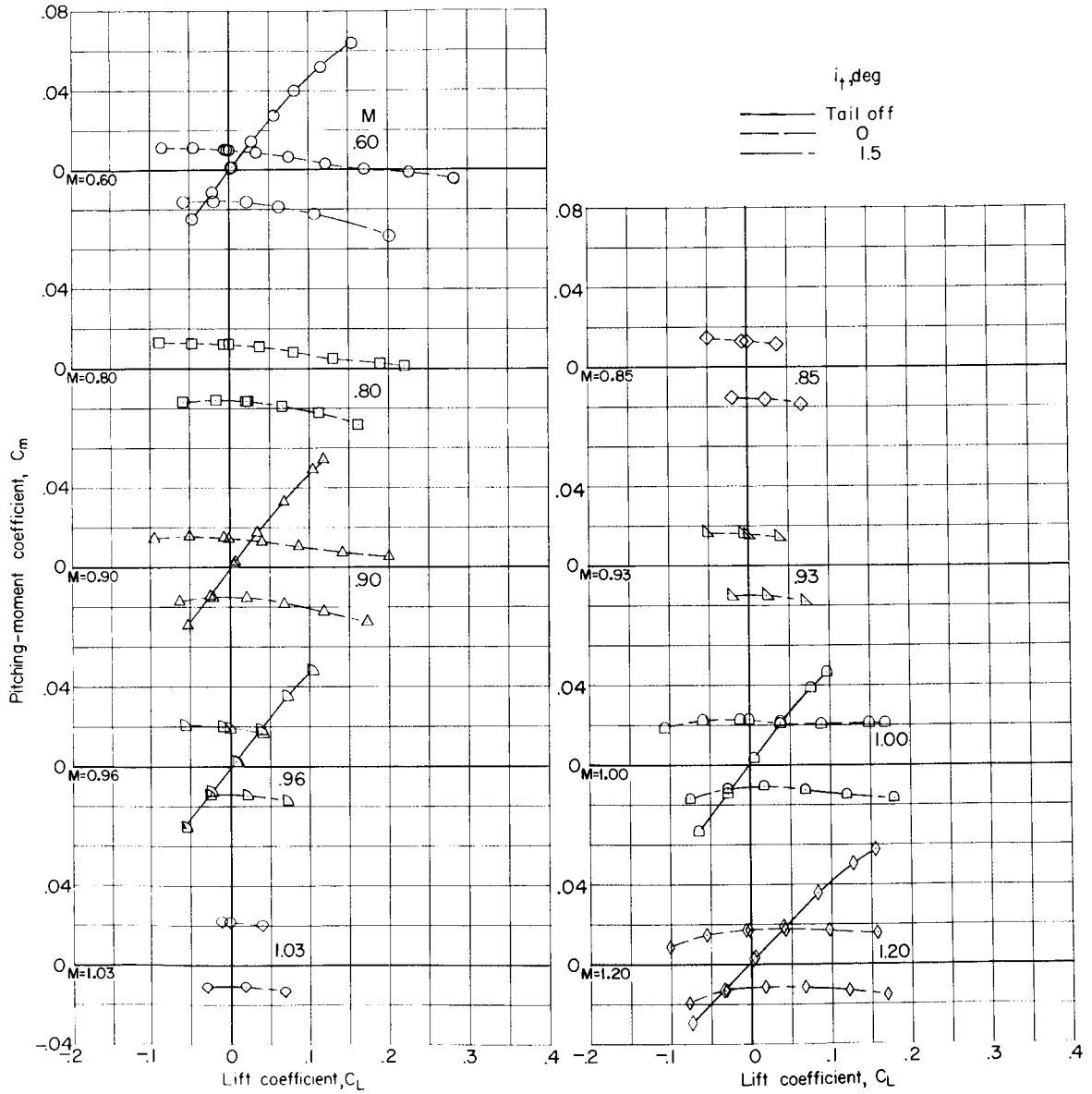
L-1170



(b) Drag coefficient.

Figure 18.- Continued.





(c) Pitching-moment coefficient.

Figure 18.- Concluded.



~~CONFIDENTIAL~~

L-1150

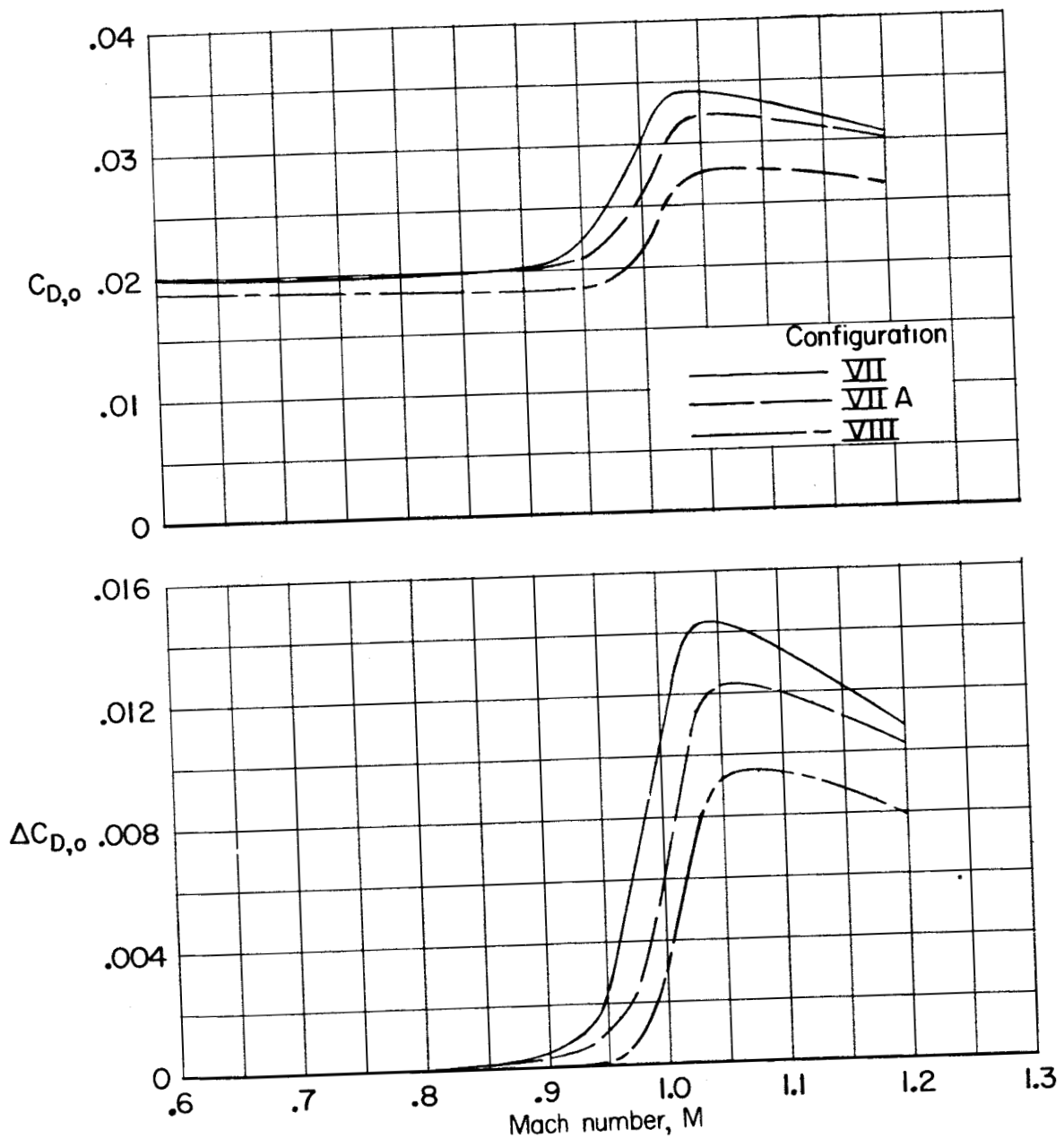


Figure 19.- Comparisons of the drag rise for the various configurations tested with maximum wing sweep.

~~CONFIDENTIAL~~

CONFIDENTIAL

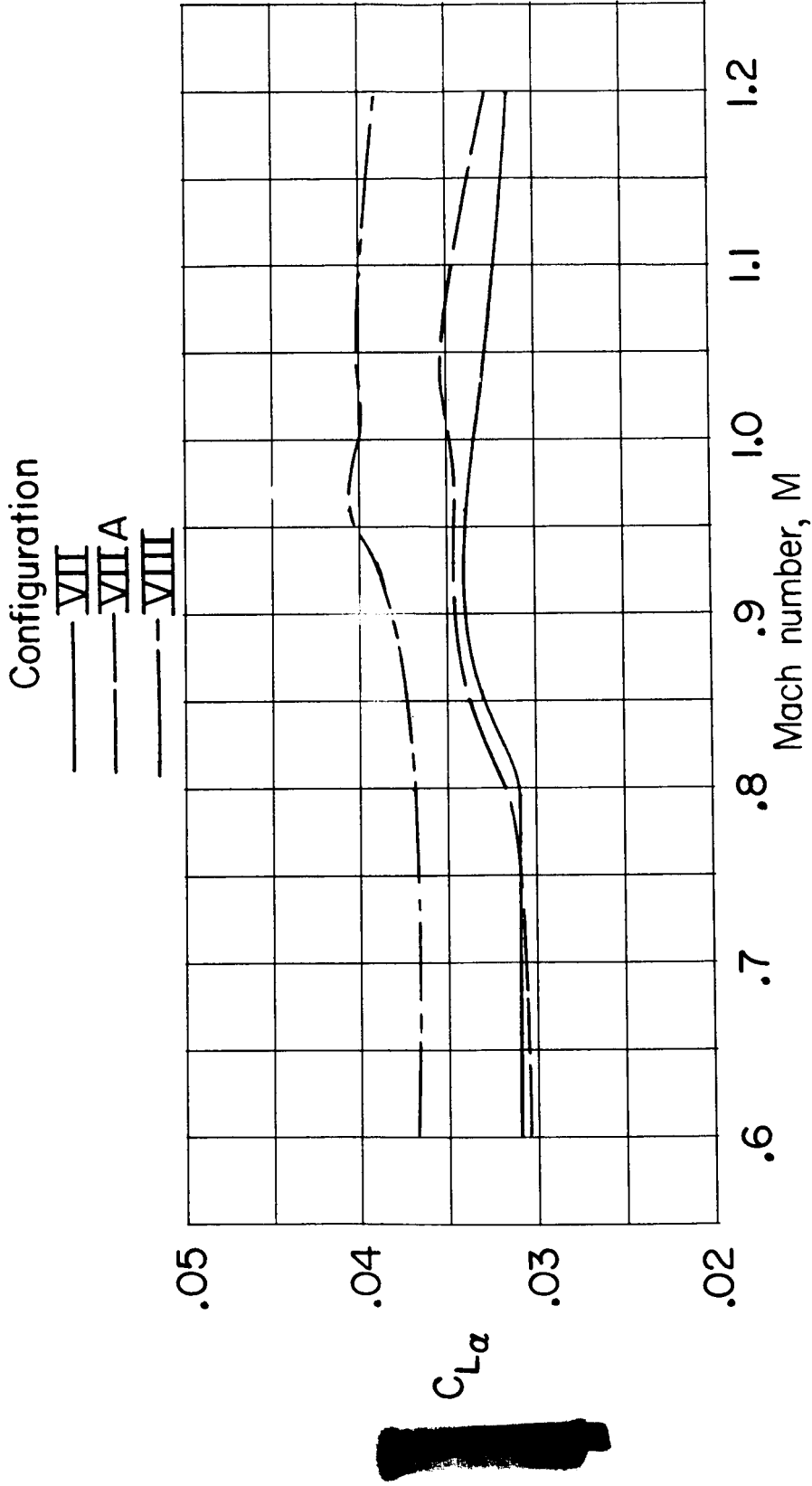


Figure 20.- A comparison of the lift-curve slopes for the various configurations tested with maximum wing sweep. $C_L = 0$.

SECRET

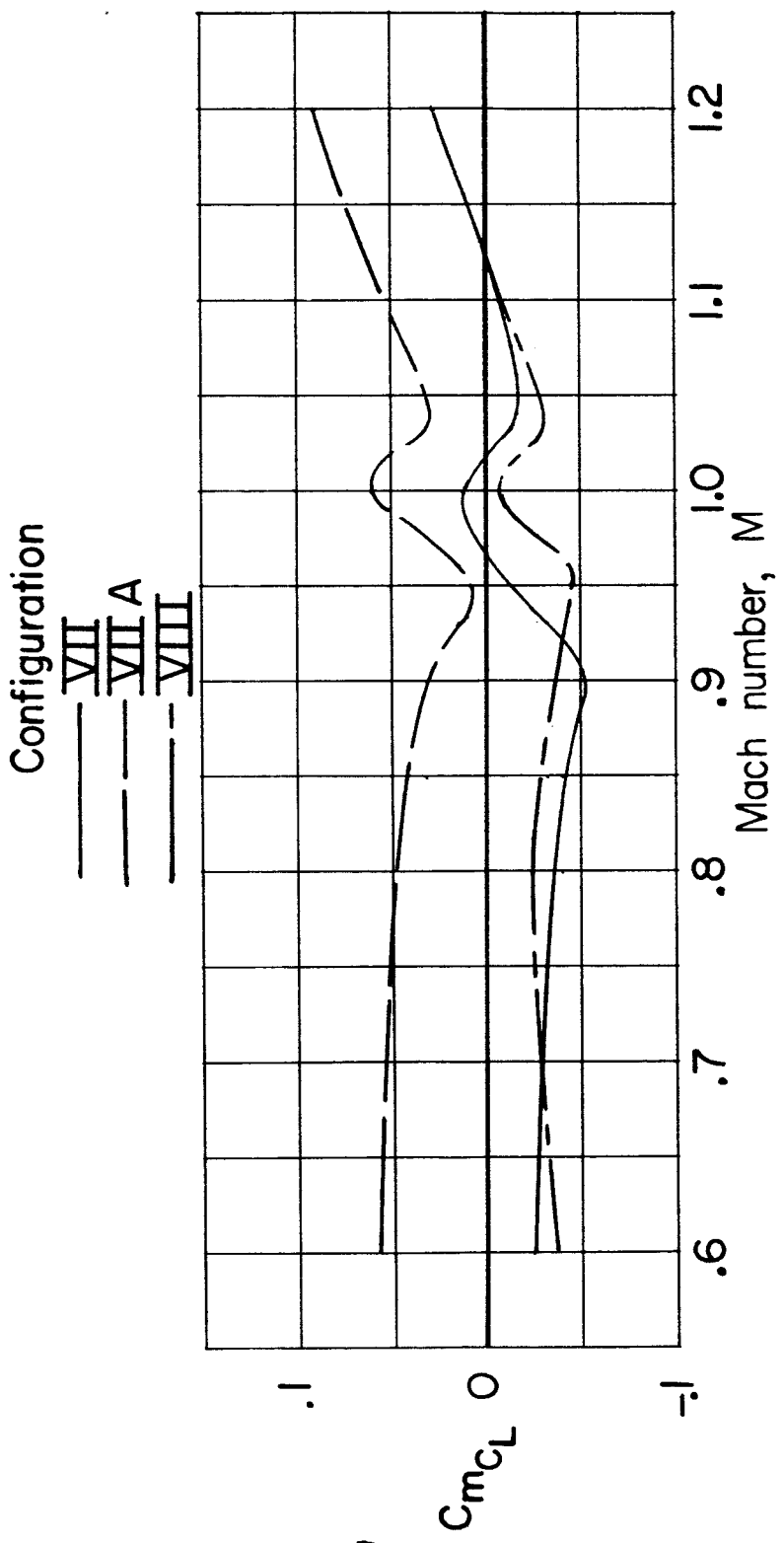
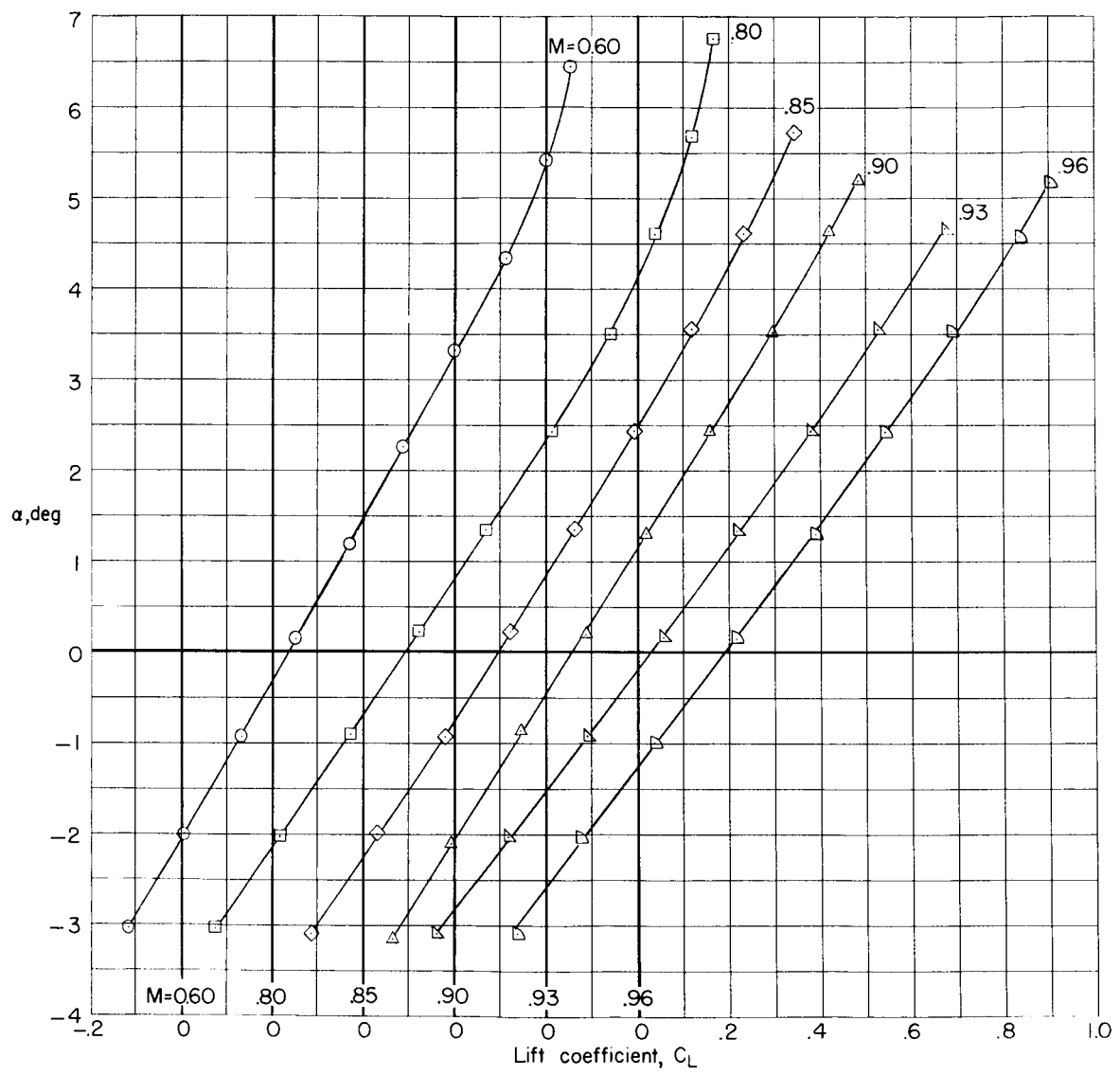
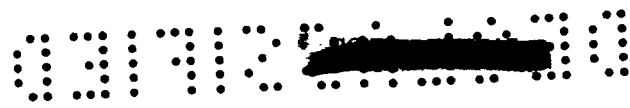


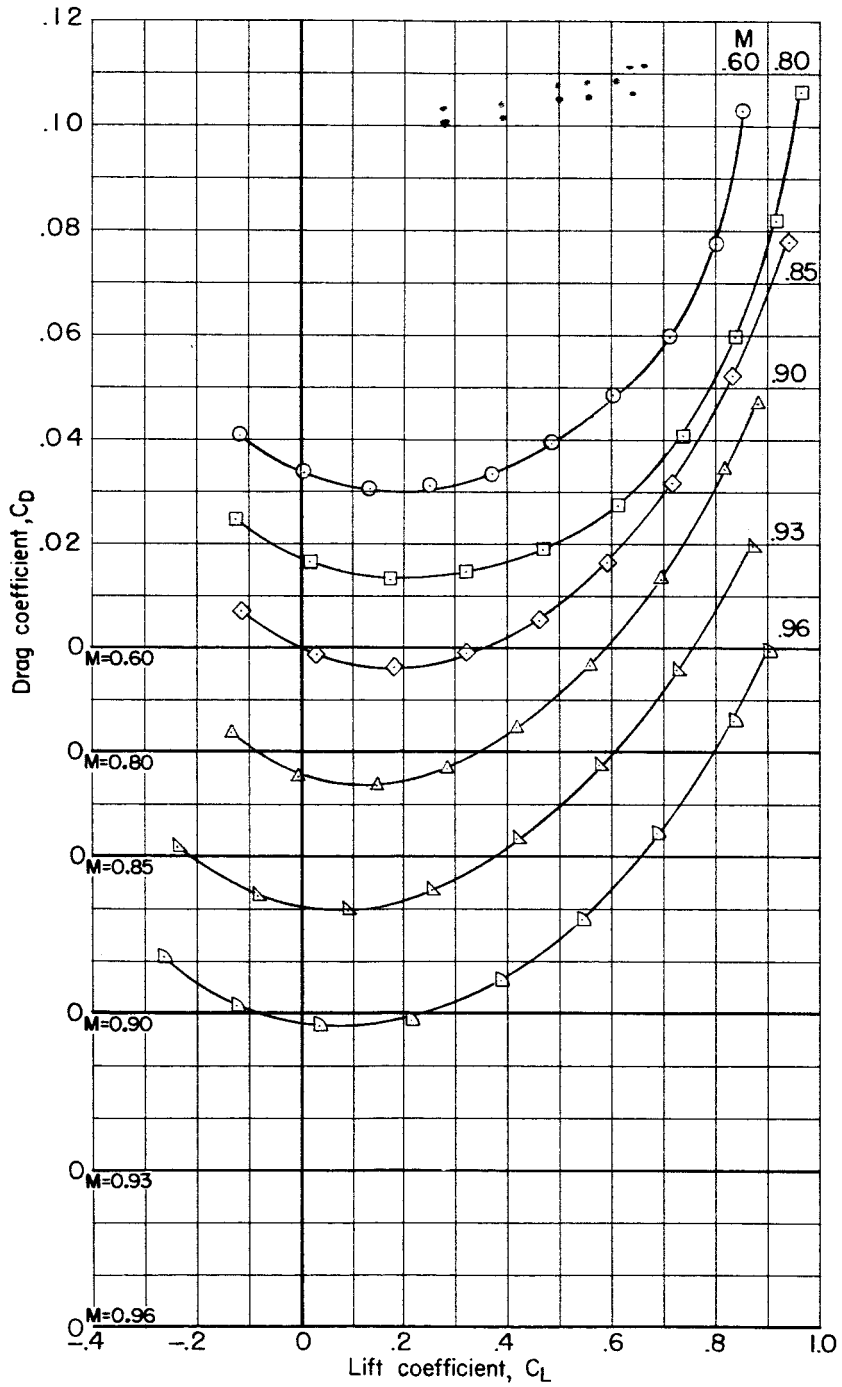
Figure 21.- A comparison of the pitching-moment-curve slopes for the various configurations tested with maximum wing sweep. $C_L = 0$.



(a) Angle of attack.

Figure 22.- Aerodynamic characteristics of configuration VIII with wing swept back 25° . $i_t = 1.5^\circ$.

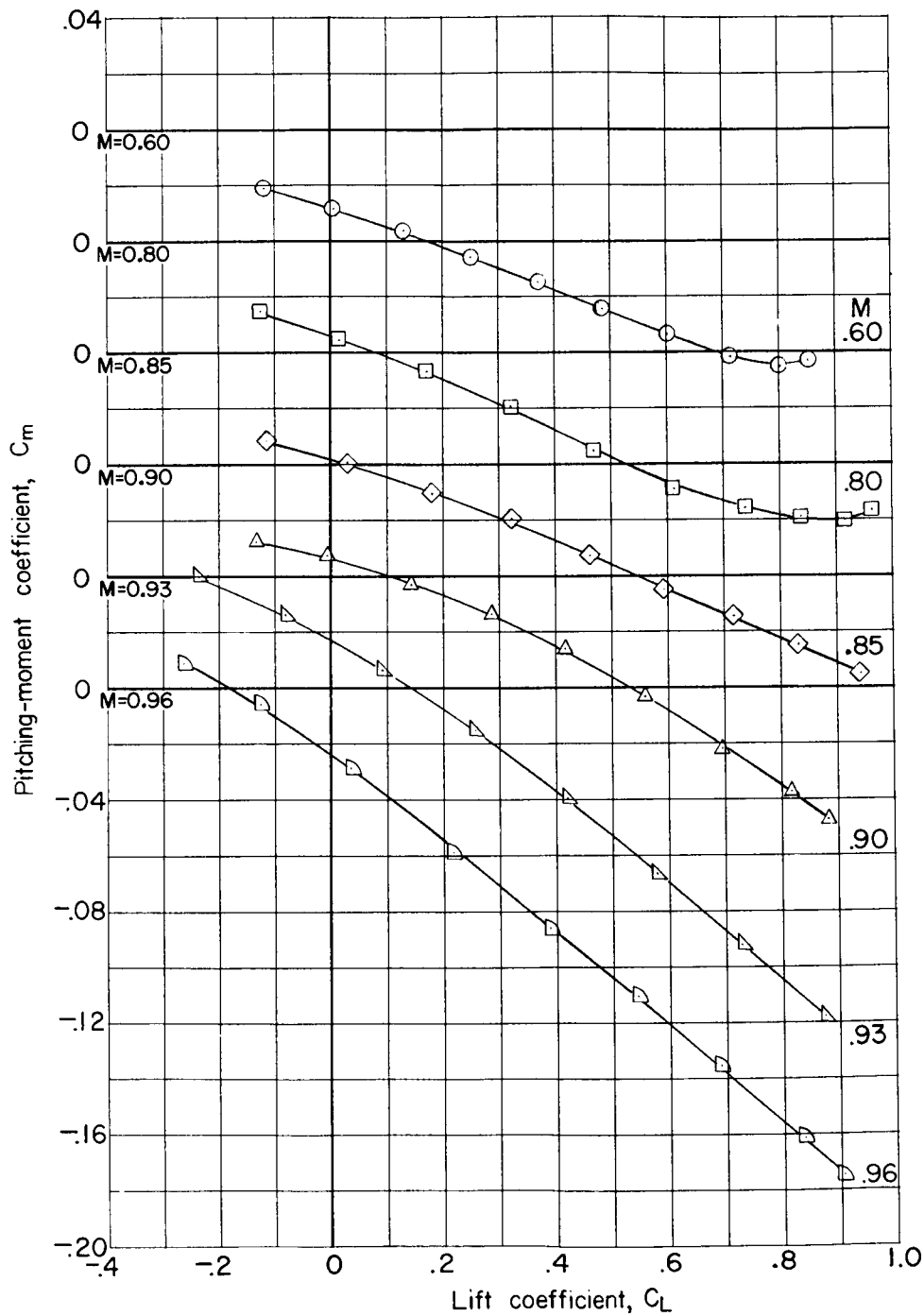




(b) Drag coefficient.

Figure 22.- Continued.

L-1150



(c) Pitching-moment coefficient.

Figure 22.- Concluded.



1-1150

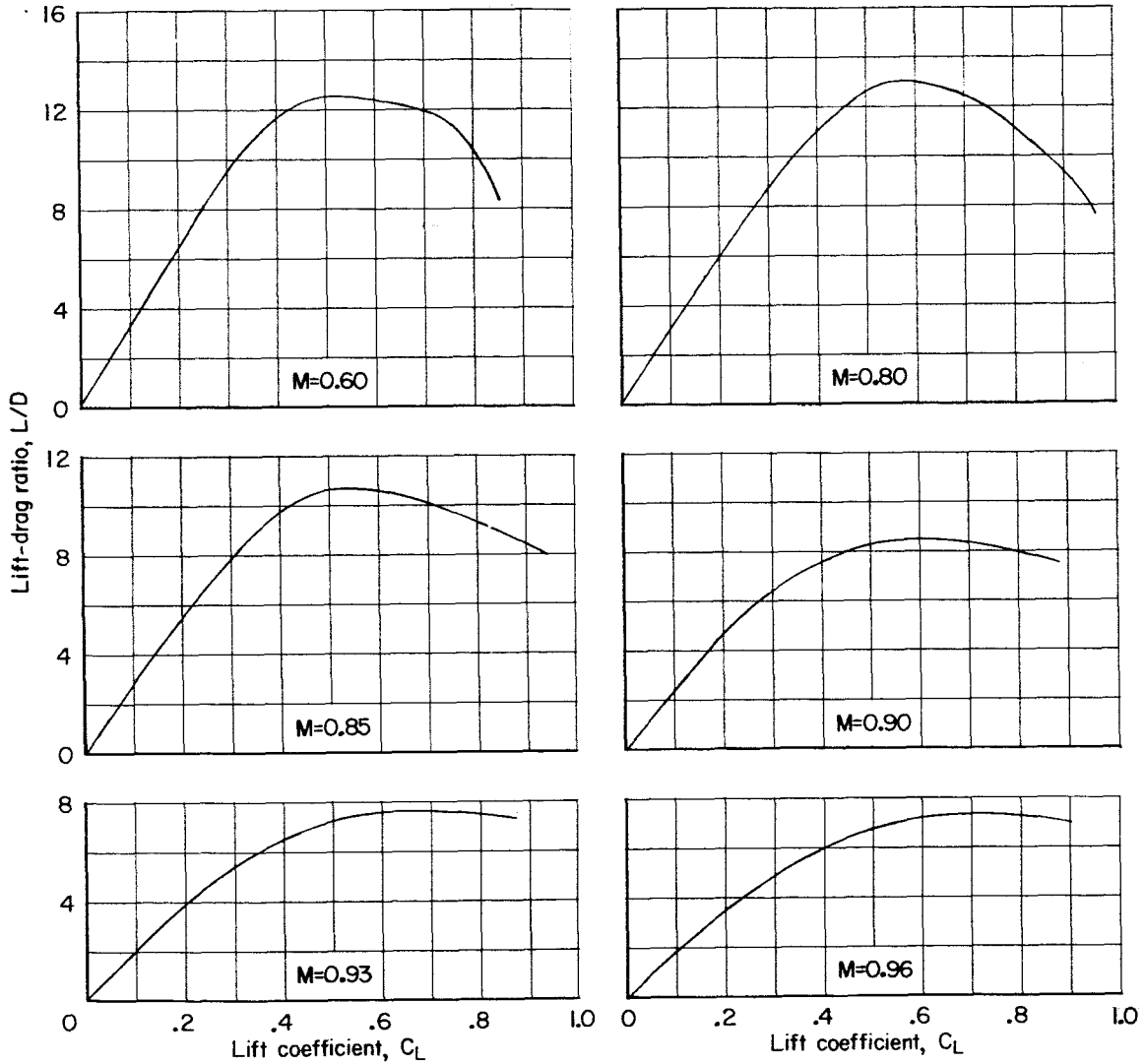


Figure 23.- Variation of the lift-drag ratio with lift coefficient at various Mach numbers for configuration VIII with wing swept back 25° .

CONFIDENTIAL

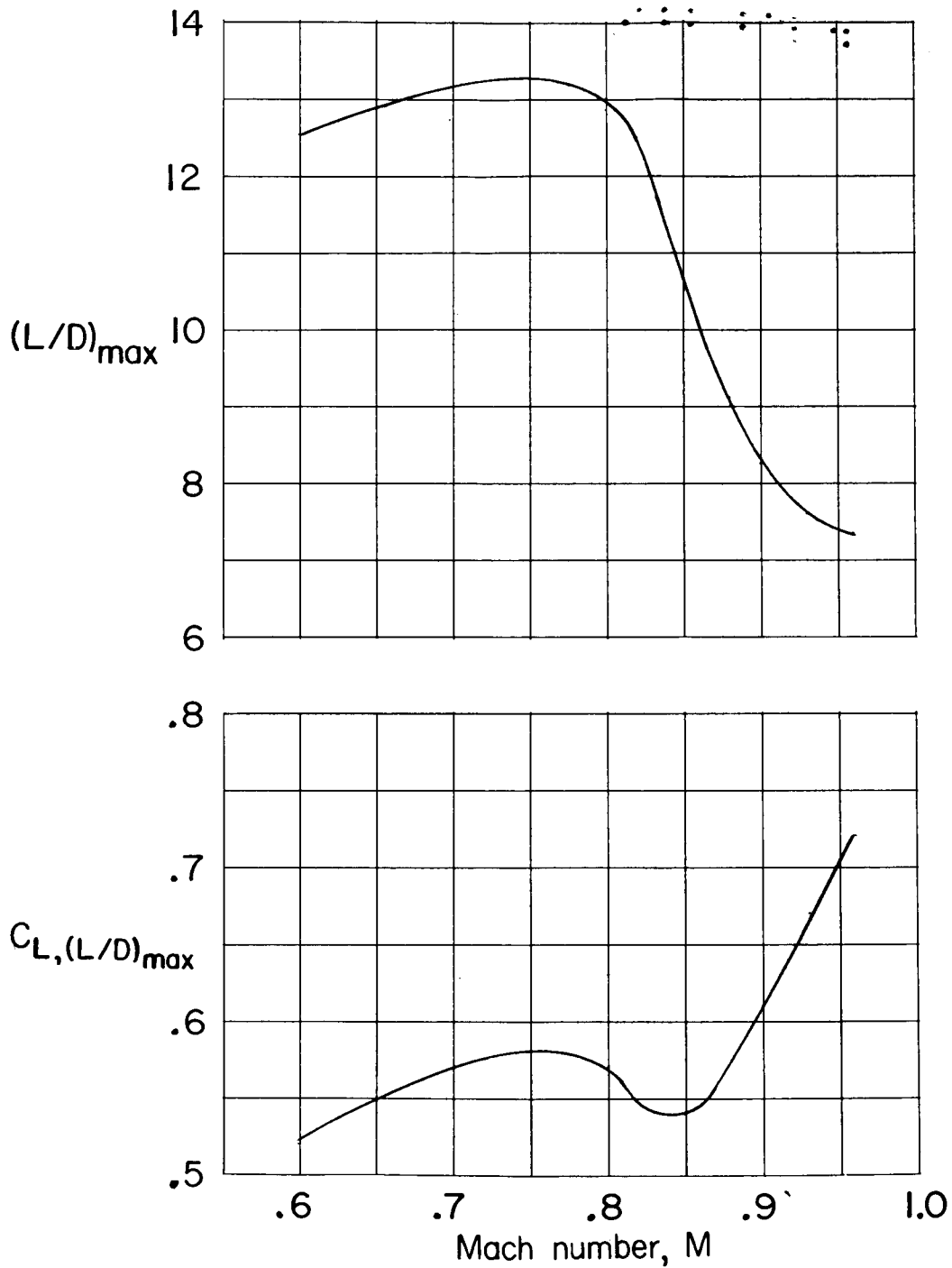


Figure 24.- Variation with Mach number of the maximum lift-drag ratio and lift coefficient for $(L/D)_{max}$ for configuration VIII with wing swept back 25° .

CONFIDENTIAL

SECRET

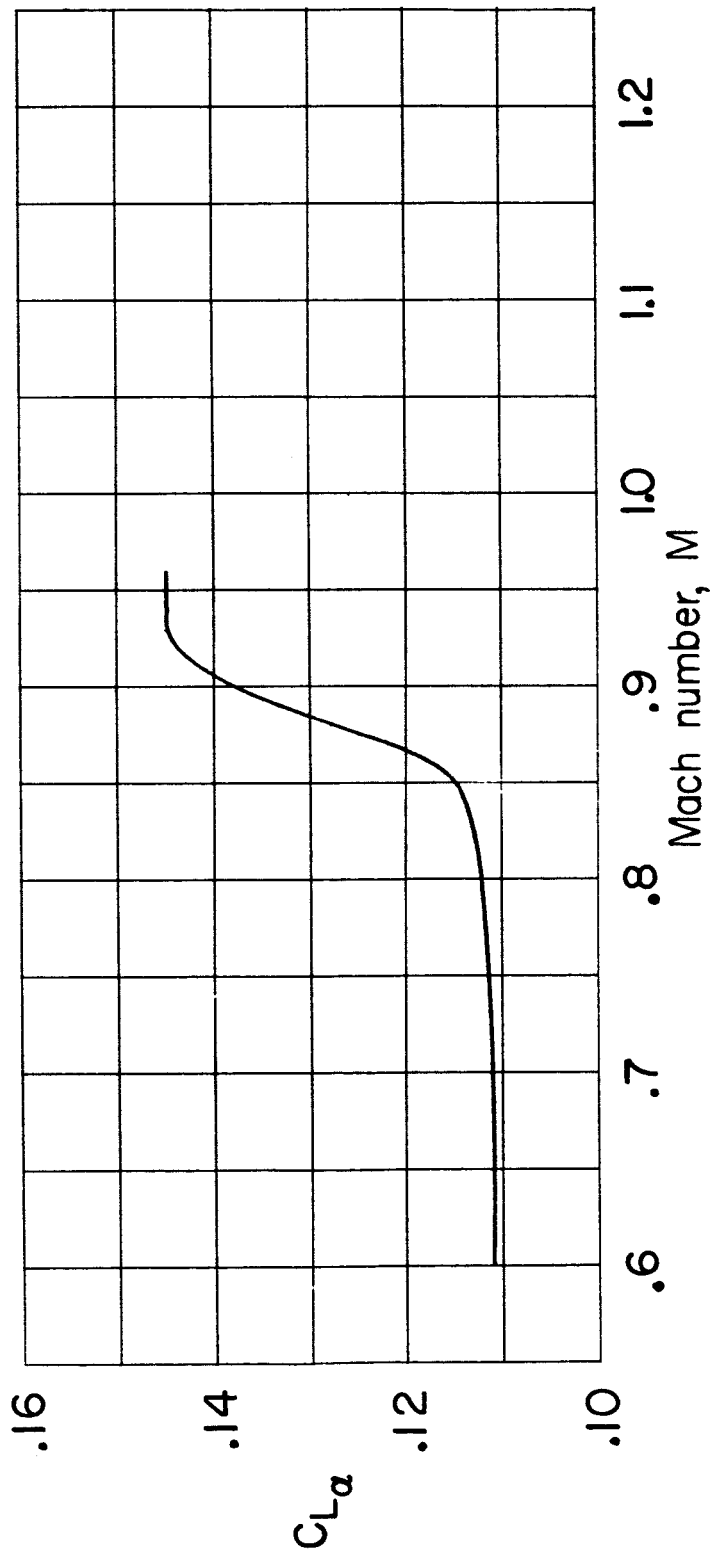


Figure 25.- Variation of the lift-curve slope with Mach number for configuration VIII with wing swept back 25°. $C_L = 0.3$.

CONFIDENTIAL

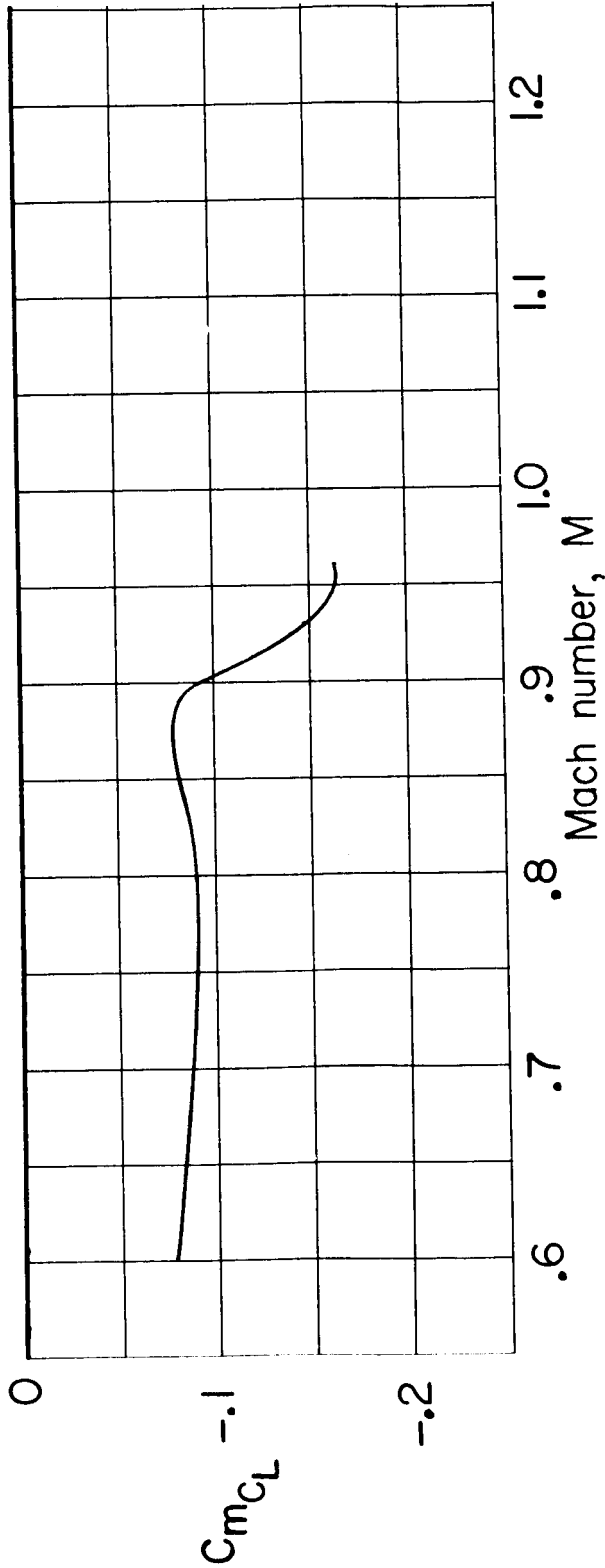


Figure 26.- Variation of the pitching-moment-curve slope with Mach number for configuration VIII with wing swept back 25°. $C_L = 0.3$.

CONFIDENTIAL